Evaluation of Texture Features For Analysis of Ovarian Follicular Development

A Thesis Submitted to the
College of Graduate Studies and Research
in Partial Fulfillment of the Requirements
for the degree of Master of Science
in the Department of Computer Science
University of Saskatchewan
Saskatoon

By
Na Bian

Permission to Use

In presenting this thesis in partial fulfilment of the requirements for a postgraduate degree from the University of Saskatchewan, I agree that the Libraries of this University may make it freely available for inspection. I further agree that permission for copying of this thesis in any manner, in whole or in part, for scholarly purposes may be granted by the professor or professors who supervised my thesis work or, in their absence, by the Head of the Department or the Dean of the College in which my thesis work was done. It is understood that any copying or publication or use of this thesis or parts thereof for financial gain shall not be allowed without my written permission. It is also understood that due recognition shall be given to me and to the University of Saskatchewan in any scholarly use which may be made of any material in my thesis.

Requests for permission to copy or to make other use of material in this thesis in whole or part should be addressed to:

Head of the Department of Computer Science
176 Thorvaldson Building
110 Science Place
University of Saskatchewan
Saskatoon, Saskatchewan
Canada
S7N 5C9

Abstract

Ovarian follicles in women are fluid-filled structures in the ovary that contain oocytes (eggs). A dominant follicle is physiologically selected and ovulates during the menstrual cycle. We examined the echotexture in ultrasonographic images of the follicle wall of dominant ovulatory follicles in women during natural menstrual cycles and dominant anovulatory follicles which developed in women using oral contraceptives (OC). Texture features of follicle wall regions of both ovulatory and anovulatory dominant follicles were evaluated over a period of seven days before ovulation (natural cycles) or peak estradiol concentrations (OC cycles). Differences in echotexture between the two classes of follicles were found for two co-occurrence matrix derived texture features and two edge-frequency based texture features. Co-occurrence energy and homogeneity were significantly lower for ovulatory follicles while edge density and edge contrast were higher for ovulatory follicles. In the each feature space, the two classes of follicle were adequately separable.

This thesis employed several statistical approaches to analyses of texture features, such as plotting method and the Mann-Kendall method. A distinct change of feature trend was detected 3 or 4 days before the day of ovulation for ovulatory follicles in the two co-occurrence matrix derived texture features and two edge-frequency-based texture features. Anovulatory follicles, exhibited the biggest variation of the feature value 3 or 4 days before the day on which dominant follicles developed to maximum size. This discovery is believed to correspond to the ovarian follicles responding to system hormonal changes leading to presumptive ovulation.

Acknowledgements

The work described in this paper was supported by Dr. Roger A. Pierson, in the Department of Obstetrics, Gynecology and Reproductive Sciences, University of Saskatchewan. Many valuable references related to this study were provided by him. All the images processed in this study were provided by the Women's Health Imaging Research Laboratory (WHIRL).

Special thanks Dr. Eramian for not only giving me the opportunity to work in this interesting research but also being a great mentor.

Thanks to my friends for either giving me suggestions or other helps during the work.

Thanks to my parents, for everything.

Finally, I wish to thank my husband for his understanding and help.

Contents

List of Tables

List of Figures

Chapter 1

Introduction

1.1 Background Knowledge about Ovarian Follicles

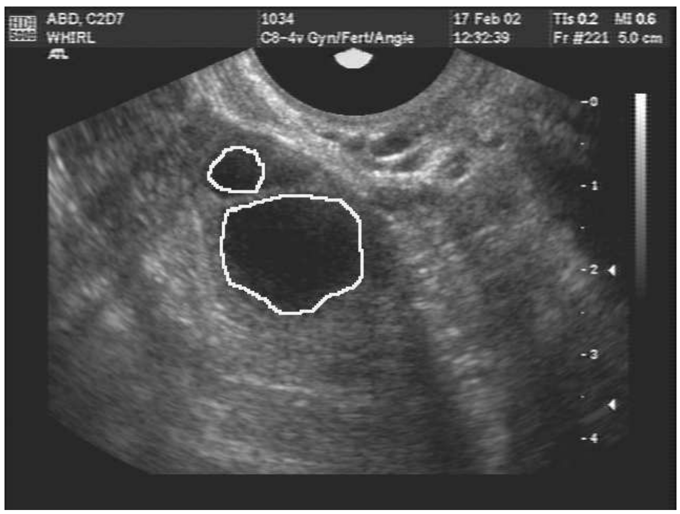

Figure 1.1: An ovarian ultrasound image with marked follicles.

The study of the development of human ovarian follicles has been of increasing interest in recent years and is a significant area of women's health. Compared with research on animal ovarian follicles, human ovarian follicles are more difficult to study due to ethiced consideration. Thus, much of the understanding of human follicular development has been based only on indirect information, such as measurements of hormones levels, including the concentrations of Leutinizing Hormone (LH), follicle stimulating hormone (FSH), estradiol, and progesterone. Because of the indirect studies in women, human ovarian function, ovulation / anovulation and follicle growth / regression are still not fully understood. Currently, ultrasonography, a widely utilized tool for non-invasive visualization of internal organs, has been used during the menstrual cycle to assess follicle growth. Figure 1.1 shows an example of an ovarian ultrasound image with two marked follicles. Ultrasonography enables collecting ovarian follicle images and performing sequential analyses in living women, thus broadening research approaches to the study of follicles.

An ovarian follicle and its development from its primordial form to its eventual demise as the corpus luteum is described in the following schematic (Figure 1.2). The top left of the figure shows the first stage of follicular maturation. Primary oocytes are surrounded by a single layer of follicular cells. As the follicle grows, an antrum and stratum granulosum cell layers begin to form. A mature ovarian follicle, shown on the bottom right of Figure 1.2, is roughly spherical in shape, with a diameter of about 23 mm. It is composed of the follicle wall (the theca interna, theca externa, and stratum granulosum cell layers, about 0.2 mm thick), enclosing a fluid interior. Ovulatory dominant follicles ovulate and then are observed as corpora lutea (see the bottom left of Figure 1.2), which is a temporary endocrine gland formed following the release of the egg.

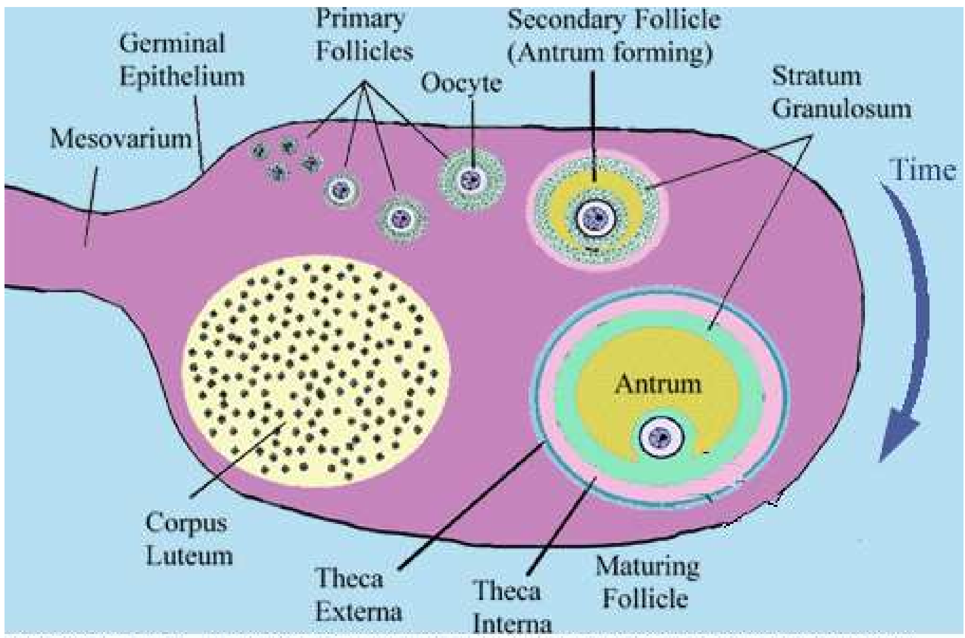

Figure 1.2: Schematic representation of ovarian follicular development over time.

The development of an ovarian follicle in women is correlated with the cyclic changes in glycoprotein hormones from the anterior pituitary [1]. Normally, at the beginning of the normal menstrual cycle, the hypothalamus releases gonadotropin-releasing hormone (GnRH) (step 1 in Figure 1.3). This hormone causes an increase in the secretion of FSH and LH from the pituitary gland, which lies at the base of the brain (step 2 in Figure 1.3). FSH and LH are carried by the bloodstream to the ovaries where they stimulate a number of ovarian follicles to grow. Once the follicles are stimulated by FSH and LH, they begin to produce estradiol (E2). Among the ovarian follicles stimulated to grow during this cycle, only one follicle is destined to ovulate. Selection of a dominant follicle is associated with a decline in concentrations of FSH and LH; thus, there is less circulating FSH and LH available to stimulate other follicles. Meanwhile, the follicle that is destined to ovulate continues to grow, producing more and more estradiol (step 3 in Figure 1.3). This is followed by a rapid increase reaching the peak E2 level (see step 6 in Figure 1.3) which causes an acute increase in LH that triggers ovulation of the dominant follicle. Following ovulation, there is an acute drop in estradiol and the collapsed follicle undergoes structural and functional transformation to the corpus luteum. Thus, the highest estradiol level appears on the day before or the day of ovulation (step 4 in Figure 1.3). The LH surge also simulates the ruptured follicle to turn into a corpus luteum (step 7 in Figure 1.3). Once the corpus luteum degenerates, FSH and LH be released from the pituitary and the cycle will begin anew.

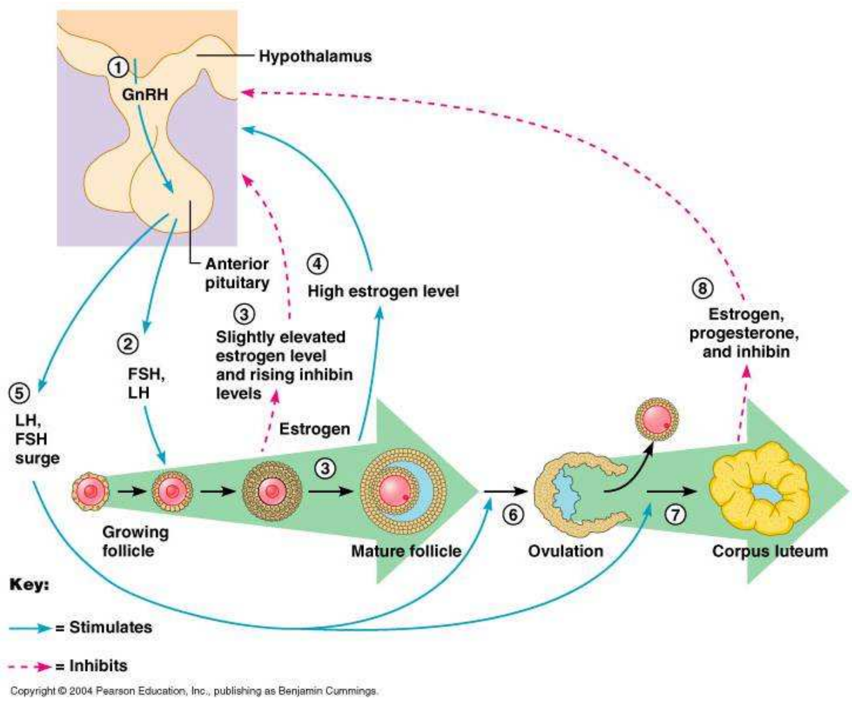

Figure 1.3: Hormones of the ovarian cycle.

Many researchers have been recently attracted to the issue of follicular development during oral contraceptive (OC) use. A number of problems in this area, such as how and when the oral contraceptives affect follicular growth, regression and hormone levels during compliant use of OC, are desired for better control and further advancement of contraceptive technology.

It is known that follicle that will ovulate has to grow to an appropriate size, called pre-ovulatory size. For example, ovulatory follicles usually have a diameter of 9 mm on the 7th day before ovulation, 14 mm on the 3rd day before ovulation and 22 mm on the day of ovulation. Among the studies of follicular development during the use of OC, a remarkable phenomenon has been discovered [2]. Some anovulatory ovarian follicles in OC users have been found to grow to pre-ovulatory size under exogenous hormonal influence and exhibit normal follicular growth although they do not ovulate. Figure 1.4 presents data from one woman showing incomplete inhibition of follicular development by OC. The x-axis denotes the day in an ovarian cycle, for example, cycle day 220 means the 20th day on the second cycle and cycle day 320 means the 20th day on the

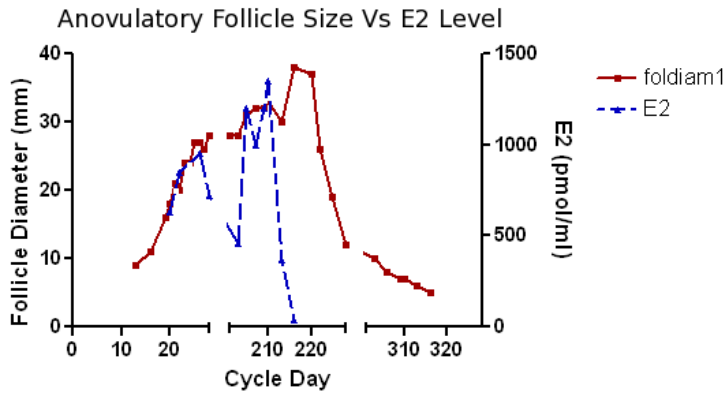

Figure 1.4: Standardized E2 level and dominant anovulatory follicle size. The anovulatory follicle grew to preovulatory sizes and experienced the peak value of E2 when it grew to the biggest size on the 20th day of 2nd cycle, it graduatly regressed on the 10th and 20th day of 3rd cycle, without ovulation.

third cycle. We note an anovulatory follicle in OC user can also grow to the potentially ovulatory size. But following the drop of E2 level, the follicle regresses without observation of ovulation. The reason why some anovulatory follicles grow but do not ovulate, is not understood.

1.2 Objectives of the Thesis

The motivation of this study is to understand the differences between ovulatory follicles in women with natural cycles, and the anovulatory follicles which grow to potentially ovulatory sizes in women taking oral contraceptives by analyzing the echotexture of the region of interest (ROI) in ultrasound images.

The follicle walls of the dominant follicles are of interest in this study. Three specific objectives for this study are:

(1) Texture features of follicle walls in ultrasound images will be extracted and analyzed by appropriate image processing approaches, which include image pre-processing of ROI, gray scale adjustment, image contour detection and texture analysis;

(2) Echotextural differences between the two classes of follicles will be measured statistically. We will try to detect the general trends of the texture features over time; and,

(3) Texture features of the two classes of dominant follicles that may be used to elucidate underlying ovarian function are identified.

The study will provide us a better understanding about the image characteristics of both ovulatory follicles and anovulatory follicles. The results may be a great contribution for the future work of ovarian follicles, including the prediction of the growth and atresia of ovarian follicles, the classification of ovulatory and anovulatory ovarian follicles, and improvement of OC effectiveness.

1.3 Literature Review

Two main approaches have been used to evaluate ovarian follicular development: non-image-processing approaches and image analysis approaches. Early studies were mainly based on non-image-processing approaches. A typical non-image-processing approach involves sampling of urine and serum endocrine levels to evaluate follicle growth and ovulation indirectly in women. This has been performed on women using OC [3, 4]. In [5], ovarian activity during regular use of oral contraceptives was assessed by ultrasonographic evaluation of follicular growth and measurements of 17-β-estradiol and progesterone. No obvious relationships between follicle sizes and the levels of E2 and progesterone were observed. It was noted that ovarian activity may be present without ovulation during OC use. These indirect approaches, however, cannot characterize the structural and physiological changes of ovarian follicles accurately.

Many image-processing based studies use high resolution transvaginal ultrasonography to visualize follicle activity and analyze image attributes. Ultrasound imaging has the benefits of being non-invasive, easy to operate and inexpensive. Therefore, the use of ultrasonographic technologies in medical image processing have become very common in the last two decades.

Successful use of image analysis and image processing approaches have been reported for a variety of applications, including studies of ovarian follicular development in domestic animals [6, 7, 8, 9] and humans [1]. The best example of impact of imaging technologies is the proof of the wave-phenomenon of ovarian follicles in cows. The wave theory of follicular development was originally proposed from observations made in the bovine species [10]. Rajakoski found two waves of follicle growth occurred during the estrous cycle based on gross evaluation of ovaries obtained from cows slaughtered on known days of the estrous cycle. This wave-phenomenon was not fully accepted until the first ultrasonographic studies of the bovine ovary [8, 11].

Ultrasound studies have been conducted on humans as a tool for clinical diagnosis and studies such as the detection and characterization of pathology. For example, it has been used to detect liver diseases [12, 13], prostate diseases [14], breast cancer [15], and diseases of the uterus [16], ovary [17] and brain [18, 19]. Besides diagnosing pathologic changes using ultrasound images, researchers have also tried to understand biological status of tissues and cells in humans by analyzing the image attributes. The study of ovarian follicular status in women has resulted in significant changes in our understanding of ovarian follicles [20, 2, 21, 22]. Singh et. al. [23] gave a good survey of image analysis techniques used in ovarian research including spot analysis, line analysis, region analysis, wavelet packet texture analysis and mathematical modeling. These varieties of techniques have been used widely in medical applications. However, they each have limitations. Spot analyses provide a mean pixel value and a standard deviation value within a selected spot in the image. Similarly, line analysis depicts the amplitude of echoes along a line drawn across a specific section of the image of the follicle. The spot and line analyses extract numerical data, but placement of the spot and line in a region free of artifacts may be difficult. Wavelet texture analysis is based on Fourier analysis. The traditional technique uses a window Fourier transform. The size of a Fourier window determines the time-frequency resolution. However, the global frequency contents of most images are not constant. To overcome the resolution limitation of a window, we use a window whose width changes as the frequency changes. This technique is computationally expensive compared to using a fixed-size window. For example, images of the follicular antrum were transformed into 85 wavelet images using only three scale levels in [24]. Sarty et al., [25] proposed a method for automatically detecting the outer follicle wall boundaries in ultrasonographic images of ovaries using prior knowledge about image edge strength and direction, typical follicle shapes, and the knowledge of follicle wall. The follicle of interest was isolated, and parameters including the size of follicle, root mean square deviations of the fluid signal, or wavelet packet energy were computed for analysis of the follicular development. Unfortunately, prior knowledge is usually difficult to obtain, especially in cases of ovarian follicle where image characterizations vary frequently with ovarian functions.

Analysis of follicle size has also been used in certain circumstances, because follicle size is one of the necessary measurements for ovarian follicular growth. Follicles destined to ovulate will continue to grow, and follicles that die without ovulation will regress. Schwartz et al. [26] and Baerwald [2] both studied ovulatory follicles by measuring the maximum follicle size in ultrasonographic images during the menstrual cycles. Broome [21] also detected enlarged follicles in women during OC and applied them in the study of follicular development. However, many studies show that follicles with the pre-ovulatory size may not ovulate, which means that follicle size is just a sign of follicular growth, but not a sign of future ovulation. Thus, assessment of follicular function only by follicle size alone is inadequate.

Texture analysis differs from other image analysis methods in that it tries to characterize echo-texture of ultrasound images which mostly can not be discriminated visually. This technique has been recognized to be a powerful tool in a variety of object segmentation and pattern recognition applications. One example application was in classification of pulmonary disease such as interstitial fibrosis in X-ray images in [27], where three types of texture features were computed based on the contrast measure, directional contrast measure and a Fourier domain energy. The best classification results were obtained using directional contrast measure. Similarly, Landeweerd and Gelseman [28] segmented different types of white blood cells in ultrasound images by extracting various statistical texture features, such as co-occurrence matrices and mean gray levels. In studies of ovarian follicular development, changes of texture attributes are believed to be reflective of the phases of follicular development. A study characterizing the echotexture of ovarian follicular structures at different phases of the follicular wave was reported by Tom et al. in [9]. Echotexture was analyzed in heifers in normal estrus cycles. Each image was digitized for echotexture analysis of the follicle wall and the follicular antrum. Mean pixel value and pixel heterogeneity were found to be different in growing and regressing of follicles. Results supported the concept that image attributes (i.e. echotexture) are related to the physiologic status of follicles. Other studies [6, 7] also found that echotexture attributes were correlated with the oocyte (i.e. egg) competence and endocrine status.

Currently most image analysis studies, especially texture analyses, are on ovarian follicles in animals. Ovarian physiological stages and related structural, and textural changes in images during natural cycles and OC cycles in women have not been critically characterized.

1.4 Structure of the Thesis

This present project is designed to analyze ultrasound follicle images using texture analysis techniques. The structure of this thesis is arranged according to the basic procedure of image texture analysis. Figure 1.5 is an overview of the steps that compose the thesis, where images of ovulatory follicles from women with natural menstrual cycles and images of follicles from women using OC are considered as two categories of data. We briefly introduce the following chapters in this thesis as follows.

Chapter 2: Methodology. This chapter presents the three main reasons why texture analysis is used in this study. Image data sets and the procedure of capturing them are introduced.

Chapter 3: Preparatory Work. This chapter proposes an appropriate image pre-processing method for increasing the accuracy of texture analysis by reducing the intensity differences among ultrasound images.

Chapter 4: Feature Extraction. Five commonly used texture description methods are described. Appropriate methods are chosen by comparisons based on our particular problem. The implementation is given at the end of the chapter to show how to extract features from images in the data sets.

Chapter 5: Feature Selection. Approach to selection of texture features are presented. Principle component analysis (PCA) is briefly introduced as a tool for dimensionality deduction of feature vectors. Features that can characterize follicular development effectively are selected.

Chapter 6: Statistical Analysis of Texture Features. Texture features are analyzed statistically. Mean differences of feature values between the two categories of follicle images are measured. The trend of a specific feature is detected. Variations during the follicular development are located by the Mann-Kendall method.

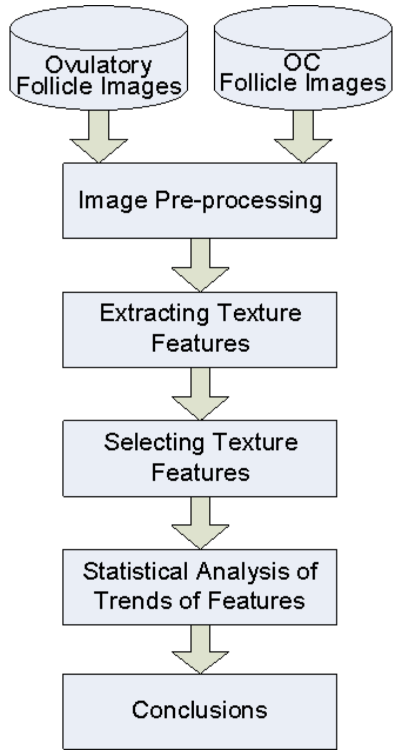

Figure 1.5: An overview of the steps composing the thesis.

Chapter 7: Conclusion. Results of this study are reviewed and potential future extensions of the project are discussed.

Chapter 2

Methodology

2.1 Justification for Use of Texture Analysis

The evaluation of ovarian follicular development for interpretation of physiologic status in women during natural cycles and during the use of OC are mainly based on texture analysis in this thesis. There are three reasons.

First, most natural organ surfaces exhibit textures; however, they can not be discriminated visually on ultrasonographic images. This is why many image analysis systems must be able to deal with the characterizing textures by texture analysis of ultrasonographic information.

Second, texture analysis techniques have been reported successful in many medical applications, including studies on ovarian follicles in animals. Basset [14] was able to discriminate various prostatic tissues (normal tissue, benign prostatic hypertrophy and cancer) using texture analyses. In studies of ovarian follicles, relationships of echotexture attributes with physiological status have been demonstrated. Sarty indicated [25] that the textures in the fluid area of ovarian follicles vary according to the stage of development of ovarian follicles in natural cycles. Follicle fluid in follicles that will ovulate have smooth, even textures and follicles that do not ovulate display rough textures. This is believed to be due to cells flaking off the follicle wall during atresia and becoming suspended in the follicle's fluid-filled interior. Therefore, texture characteristic of the follicle fluid area may be a significant feature used for detection of physiological status of ovarian follicles.

Third, current studies on human ovarian follicles focus only on a small number of topics using limited techniques. Topics such as prohibitive influence of oral contraception and the correlated biological development of ovarian follicles, are desired to understood.

This thesis is designed to compare image attributes of both ovulatory follicles and anovulatory follicles by means of texture analysis. Results of the evaluation may be fundamental to other research about human ovarian activity.

2.2 Materials and Methods

All ultrasound ovarian follicle images used in the thesis study were provided by the Women's Health Imaging Research Laboratory (WHIRL), in the Department of Obstetrics, Gynecology and Reproductive Sciences at the University of Saskatchewan.

Eight series of images from women with normal menstrual cycles were analyzed. Each series consisted of 6 to 8 images of a single ovarian follicle imaged beginning several days prior to ovulation and ending on the day of ovulation. A second series of seven dominant anovulatory follicles from women using OC were also analyzed. Each of the series consisted of 3 to 8 images of single follicles beginning several days before the characteristic peak of estradiol (E2) that would occur just prior to ovulation and ending when the sharp decline in estradiol was observed. All 15 sets of images were acquired using the same equipment and techniques [1, 2]. In total, there were 57 ultrasound ovarian follicle images in the natural cycle data set and 34 follicle images in the OC cycle data set. The number of sample images collected everyday for each category of follicles is presented in Figure 2.1. Since the absolute contrast and gray level ranges of the ultrasound images are affected by the

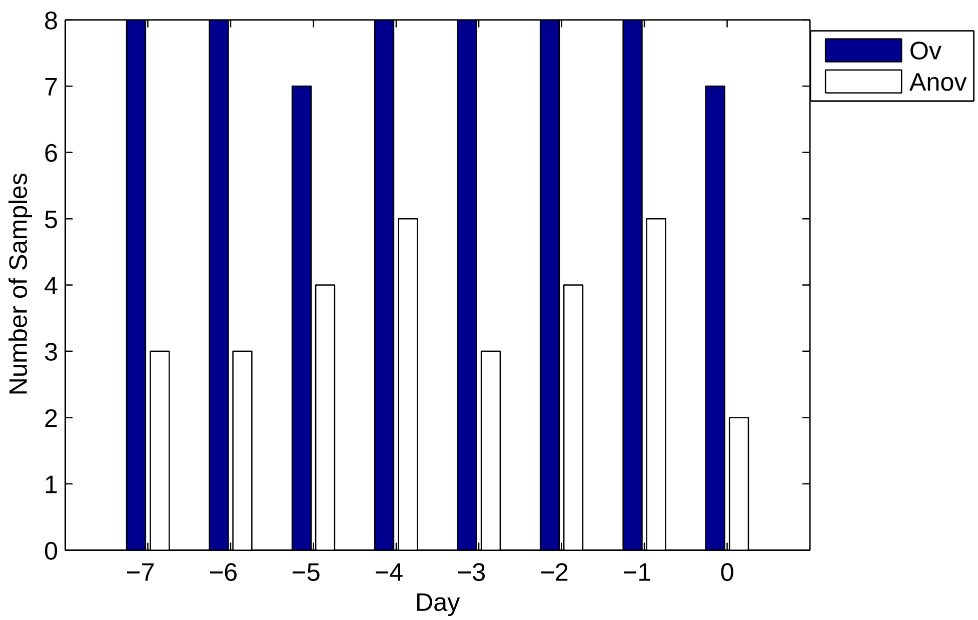

Figure 2.1: The number of sample images on each day from two groups of data.

pulse echo responses of the transducer, the transmitting frequency of the probe, random noise, and the lateral resolution of equipments, it is reasonable to compare texture features only in images acquired from the same equipment.

Hormonal data (i.e., E2 levels) and follicle diameter data from the anovulatory cycle group were provided. The E2 peak was used to align the OC series with the natural cycle series by aligning the E2 peak in OC series with the day of ovulation in the natural cycle series.

Image texture analysis techniques will be employed in evaluation of the ovarian follicular development. The original images were 640×480 pixels arrays with a dynamic range of 256 gray levels. In this thesis, we assessed follicle wall texture. The follicle wall is a thin area around the follicle antrum which is the dark interior part in the ultrasound images. To extract texture features from follicle walls, we selected them by hand based on the follicle wall contour information and object segmentation. Rough segmentation was obtained by the EDISON System v1.1 (Edge Detection and Image Segmentation) [29]. The resulting images were black in background while the gray levels of follicle walls remained unchanged.

Visual evaluation of the variations of texture features was achieved by plotting texture feature values over time for each follicle wall image. Values of each feature for all series of images were plotted on one graph along the time axis. A number of features which were able to effectively classify the ovulatory follicles in natural cycles and anovulatory follicles in OC cycles were selected based on the comparison of successful classification rate. This step reduced the number of features that were considered in later analyses of texture features. The performance of reduction of feature vectors can be improved by using prior knowledges about ovulatory and anovulatory follicles. Many previous studies provided some useful prior knowledge. For example, we know that portions of the follicle wall get thinner as ovulation appearances. In the future work, we will try to utilize more and more such information.

Finally, a number of statistical methods including means, averages, the standard deviation and statistical tests were utilized for trend analysis of each selected feature. The Mann-Kendall method, which is a powerful statistical tool and has seen much use in meteorology, was employed to detect variations in texture features and test the presence of turning points (details in section 6.2). Turning points were located and regarded as a sign of physiological change in the ovarian follicles.

Chapter 3

Preparatory Work

3.1 Ultrasound Imaging Techniques in Medical Research

Despite the extensive use of ultrasonographic imaging in medicine, the analysis of such images are significantly restricted to visual examination due to level of noise in the images. The quality of ultrasound images is often restricted to the physical nature of the imaging system. It is attributed to speckle noise in the field and the multiple reflections of the transmitted ultrasound waves, caused by coherent summation of the backscattering of the incident wave after it hits the interfaces of tissues of different acoustic impedances [30]. Alternatively, ultrasound images are created by quantitative transformation of the ultrasound wave signals to digital images. This transformation results in large amount of quantitative noises in the images. While some studies were focused on discrimination of different defects in ultrasound images [31], we only utilized images captured from the same equipment and were able to ignore the effects of system setting on the qualities of images in the present study. However, noise in ultrasound images still has to be considered. To improve the accuracy of image analyses, ultrasound images should be pre-processed to remove random noise and minimize differences of gray level contrast among images or selected areas of the images.

3.2 Image Pre-processing

The aim of image pre-processing is an improvement of the image data that removes unwanted noises or enhances some features of a region important for further processing. Our pre-processing was composed of the selection of region of interest (ROI) and gray level adjustment for the region. The follicle wall is of interest in this study. Selection of follicle wall was mainly achieved by the knowledge of object contour and image segmentation. Gray level adjustment was used for remapping the gray level values of the ROI into the same range 0 to 255. A complete procedure of image pre-processing is presented in Figure 3.1. Pre-processing methods are described in detail in section 3.2.1 and section 3.2.2.

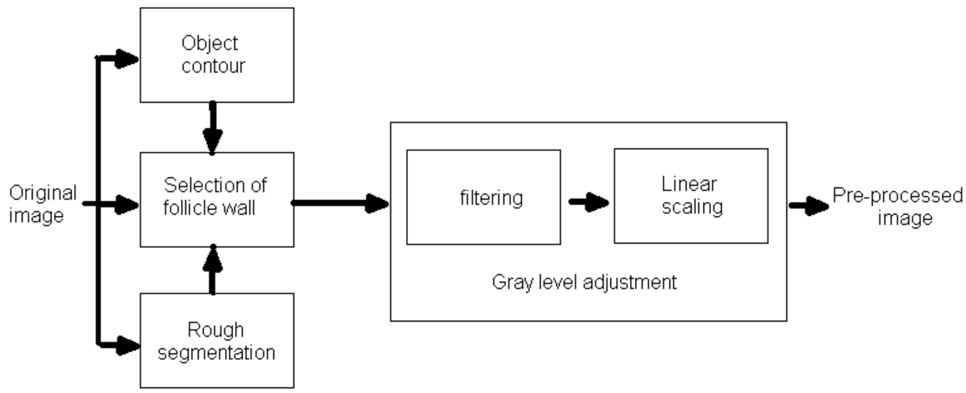

Figure 3.1: Procedure of image pre-processing.

3.2.1 Selection of Follicle Walls

The follicle wall is hard to recognize visually in ultrasound images. The follicle wall must first be recognized and isolated before we can compute texture features from it. In an ideal case, a complete segmentation may be obtained in which objects are recognized by segmenting an image into corresponding disjoint regions. However, it is difficult to achieve because a complete segmentation must use specific knowledge of problem domain. Therefore, defining and isolating objects are mostly based on partial segmentation. Commonly used methods include edge detection, object contour, and image segmentation.

Edge detection is a common way to isolate objects in an image. Edges are composed of pixels where abrupt changes (brightness) in the intensity images are found. Commonly used edge detectors include Sobel, Robert, Canny, and the Laplacian of Gaussian operator. To illustrate, we applied Canny and Laplacian of Gaussian operators on an ultrasound image. The results are shown in Figure 3.2. Discontinuous edges for the single follicle were obtained due to the edge operator's high sensitivity to noise. The whole ovarian follicle can not be accurately isolated from the derived edge images because of the absence of a single continuous boundary. Object recognition by contour can be performed using manual outlining of the object by a human operator. However, this work must be done by experts in the specific medical application. It is also time-consuming, inaccurate, and not reproducible. Full automatic contouring technique is fast in implementation, but lacks the accuracy required for many medical applications. Moreover, the size and shape of an ovarian follicle changes over time, which increases the difficulty of full automatic contouring over a time series of images. In some cases where only simple objects are analyzed, the object recognition may be achieved using full automatic contouring.

In this study, a combination of manual and automatic contouring was used. An automatic searching for contour was first applied followed by manual selection of the regions of interest from the contour image. Looking at an original ultrasound image (Figure 3.3 (a)) and its contour image

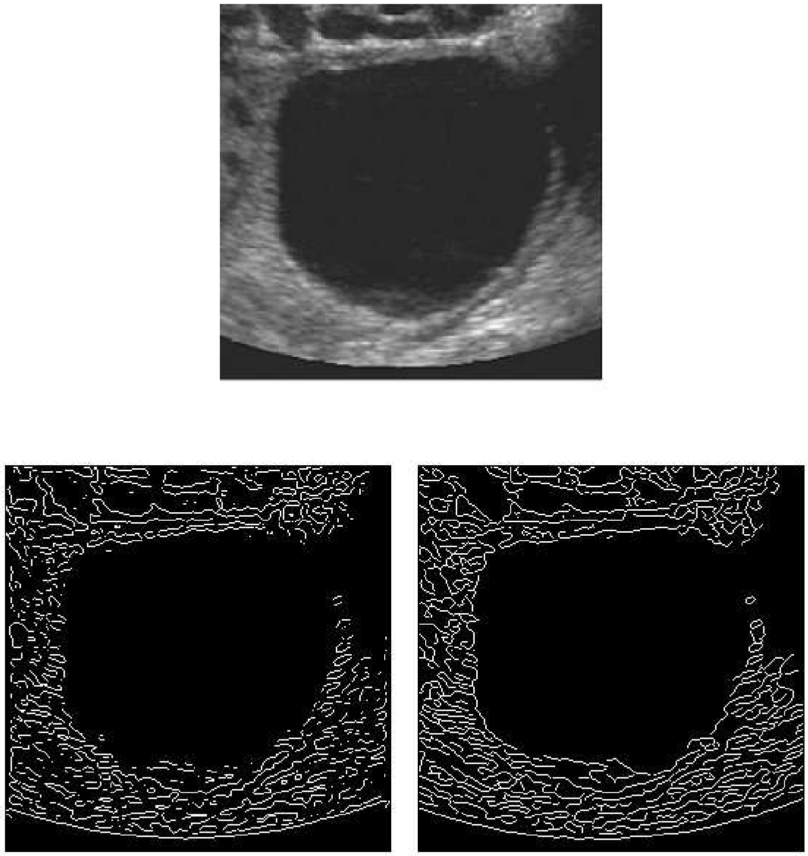

Figure 3.2: Boundary detection by edge operators. Images from top to bottom, left to right are orginal ovarian follicle image, edge image detected by Laplace of Gaussian operator, edge image detected by Canny operator.

(Figure 3.3 (b)). The contours of images were automatically generated using the image processing toolbox of MATLAB 7.0. A set of closed contour lines, as well as the gray level value of each contour line, are presented on the contour image. We can approximately locate the inner and outer follicle wall by two contours around the follicle. For example, in Figure 3.3 (b), the contour L represents the outline of inner follicle wall and contour H is the outer follicle wall. The region between them is the preliminary follicle wall. For illustration, suppose the gray level values of the inner and outer contours are A and B ($A < B$), respectively. C denotes gray level values of the thresholded image. The thresholding works as:

$$C = \begin{cases} C & A < C < B \\ 0 & otherwise \end{cases} \tag{3.1}$$

For all the pixels in the image that have gray level values higher than the lower bound (i.e. A) and lower than the higher bound (i.e. B) are kept unchanged. All the other pixels in the image with gray level values outside these two thresholds are ignored by setting their gray levels to black.

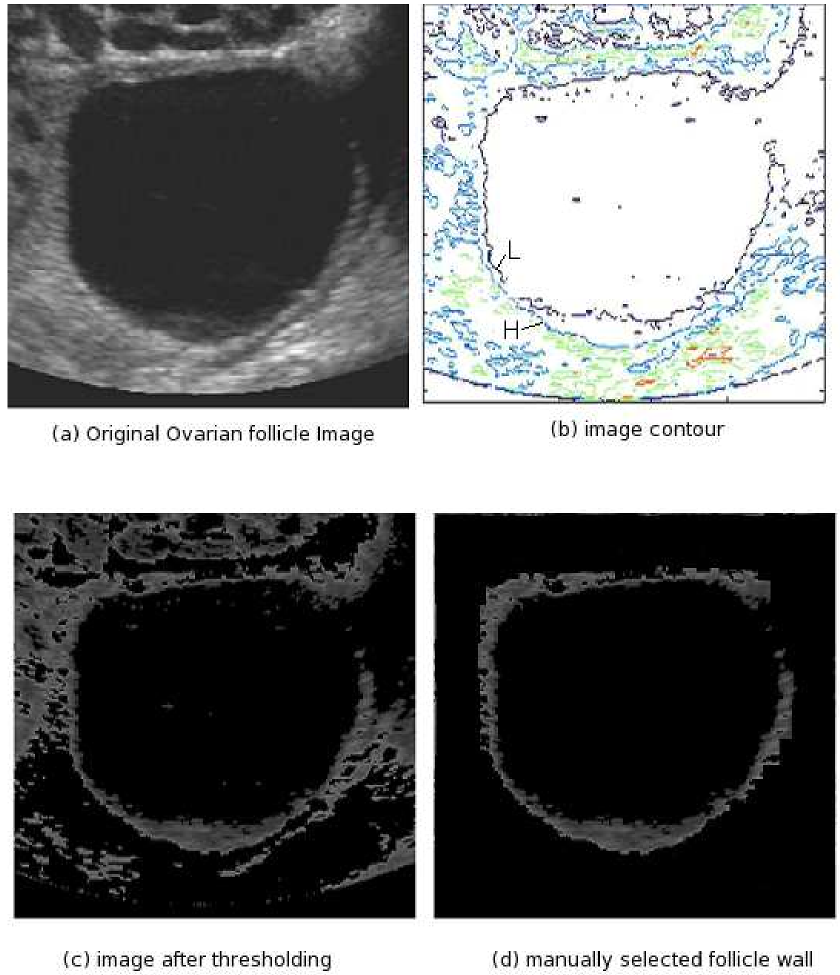

(a) Original Ovarian follicle Image (b) image contour

(c) image after thresholding (d) manually selected follicle wall

Figure 3.3: Procedure of the selection of follicle wall. Image (b) is obtained from the original image (a), gray levels of follicle contours are used as thresholds to segment (a) into (c), follicle wall in (d) is manually selected according to the information of edges and regions in (b) and (c)

To select follicle walls, we first segmented the original image using the two thresholds A and B (Figure 3.3 (c)). The resulted image contained not only follicle wall but also some other parts which had gray level values between the two thresholds. We know that the follicle wall is a thin layer of tissue around the follicle fluid which is the interior dark part in the ultrasound images. Therefore, only the area surrounding the interior black part of a follicle is selected as follicle wall, the areas outside the preliminary follicle walls, as well as regions representing isolated noises within the follicle are erased. Figure 3.3 (d) represents the resulting follicle wall obtained by manually editing image in Figure 3.3 (c). The follicle wall images obtained are black in background while the gray levels of follicle walls remain unchanged. We find that the resulting follicle walls are not perfectly round and may be discontinuous because some parts of the follicle wall may become thinner as ovulation appearances become of image artifact.

The more prior knowledge are used in manual selection, the more accurate the results will be because the method of hand-selection is not as accurate as automatic selection. Since the follicle wall region should be homogeneous in the image due to its microanatomic structure, thus if the hand-selected follicle wall is a region which is labeled to be homogeneous in an image, we can regard it as a correct selection. Otherwise, the hand-selection is considered to be inaccurate.

The segmentation of regions was achieved by employing a software, the EDISON System v1.1 (Edge Detection and Image Segmentation) because it is able to roughly segment the original image into separate regions that are homogeneous with respect to the detected edge boundaries. Homogeneity of a textural image is defined in EDISON as similarity in mean grey level values. Segmentation of homogeneous regions is achieved by assigning pixels with similar gray values and within a given boundary to a single region. Thresholds used to assign pixels are user-defined according to particular images. Each image may have different threshold in segmentation. Because this algorithm performs partial segmentations of objects based on edge detection and synergistic image segmentation, regions may not correspond directly with image objects.

The method for isolating objects on the images is dependent on specific applications. Our approach is a combination of the edge detection methods, object contour and image segmentation methods. We first locate a rough range for the follicle wall by edge detection, object contour and segmentation. The region of follicle wall is then selected by hand according to the follicle wall contours. Results of this study show that this approach is appropriate and useful for separation of homogeneous follicle walls with respect to the brightness.

3.2.2 Gray Level Adjustment

The direct comparison of image properties such as brightness, texture and color may result in an inaccurate conclusion because each series of original images in this study has different absolute gray level contrasts due to the effect of random noise. The purpose of gray level adjustment is to scale the images or follicle wall region into the same gray level range in order to obtain a set of images with uniform ranges of gray level values. The use of gray level adjustment often depends on the texture description methods used for the extraction of texture features.

Four categories of texture description approaches and their combinations are commonly used for extracting texture features. They are statistical approaches, model-based approaches, syntactic approaches, and signal processing approaches. Model-based approaches view an image texture as a set of subpatterns placed according to given rules. Textures are constructed from a model describing these subpatterns and displacement rules. Syntactic texture description is based on an analogy between the texture primitive spatial relations and the structure of a formal language. Signal processing approaches filter the image pixel by pixel with a bank of filters and then extract texture features from the filtered images. Statistical methods analyze the spatial distribution of gray values, by computing local features at each point in the image. Statistical methods can be further classified into first-order, second-order and higher-order statistics. The basic difference is that first-order statistics estimate properties (e.g. average and variance) of individual pixel values, ignoring the spatial interaction between image pixels, whereas second- and higher-order statistics estimate spatial properties of texture. Among the four categories of texture description approaches, only model-based, syntactic, and second- and higher-order statistics methods are not dependent on the absolute gray level value of each texture primitive.

The first-order statistics and signal processing methods deal with gray levels of individual pixels of an image. This means that when first-order statistics and signal processing methods are used to extract texture features, the gray level value of each pixel should not be scaled or changed in any case by any image pre-processing, otherwise the obtained texture features are meaningless and not corresponding to the original images. In this case, gray level adjustment procedure is no longer necessary. However, when other texture description approaches are used, the absolute gray level values of each primitive are not taken into account except that the spatial relationship of texture primitives should be kept unchanged. Detailed introductions of these four categories of texture description approaches involving definitions, deduction, and features computations are presented in Chapter 4.

There are many ways to implement the gray level adjustment according to the properties of considered images and aims of specific applications. We used a method for gray level adjustment to obtain the pre-processed images from which a number of second-order features were computed.

The basic procedure of the gray level adjustment used is as follows. After the follicle wall areas are selected (as stated in 3.2.1), we obtain an image I (shown in Figure 3.3 (d)) in which only the follicle wall is presented and all background pixels are set to black (i.e. gray level 0). Then a filtering operator for gray level adjustment is constructed. The complete operator is shown in Figure 3.4.

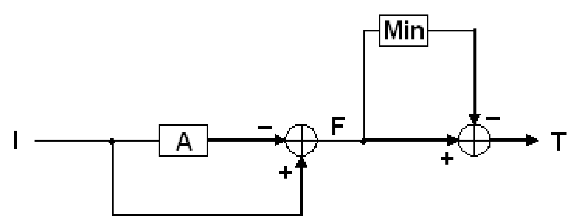

Figure 3.4: The complete filtering operator.

First, the average of the original image is subtracted from the original image I, and the filtered follicle wall image F is obtained :

$$F = I - A * I \tag{3.2}$$

where A is a $(2n + 1) \times (2n + 1)$ averaging filter, $n = 1, 2, ...$ Here a small averaging filter with size of 3×3 is chosen, because the area considered is the follicle wall which is very thin, being approximately two or three pixels wide.

Then, the image F is scanned to find the lowest pixel values present in the image, say $min(F)$. The lowest pixel values are subtracted from the image F:

$$T = F - min(F) \tag{3.3}$$

The pixel values of image T are in the interval $[0, a]$.

Finally, a gray-level values re-scaling is performed. The rescaling attempts to improve the contrast in the image by scaling the range of intensity values it contains (i.e. $[0, a]$) to the full range of pixel values, that is, the gray levels 0 to 255. Each pixel P in the image T is linearly scaled using the following function:

$$P_{out} = P_{in} * \frac{255}{a} \tag{3.4}$$

3.3 Summary

Texture analysis was not applied to the whole ultrasound image, but only to a selected region of interest (i.e. the follicle wall of dominant follicles). We first selected follicle wall region of dominant follicle from each ultrasound ovarian image. The selected follicle wall regions were processed to obtain consistent contrast ranges by removing low intensity variations with a gray level adjustment filter. Pixel gray levels of the resulting image were then linearly scaled into the range of 0 to 255.

Chapter 4

Feature Extraction

The main aim of texture feature extraction is to recognize texture properties of ovarian follicles in ultrasound images, such as fineness, coarseness, homogeneity, smoothness, regularity, linearity, frequency, and so on. This chapter first introduces five categories of commonly used texture description methods in the section 4.1. A brief comparison of all the methods are given in section 4.2. Only a few methods are employed for our particular problem to extract features from the images in our data sets. The detailed procedure of feature extraction is described in section 4.3.

4.1 Review of Methods for Texture Feature Extraction

4.1.1 Statistical Methods

Statistical texture description methods define texture based on describing the spatial distribution of gray values. The simplest statistics are the gray level first-order statistics. They describe the gray level histogram of an image. Second-order statistics such as the co-occurrence matrices and the gray level difference method describe spatial relationships between image pixels. Higher order statistics, including run length measures and the autocorrelation function, can also be measured for texture analysis. In the following sections, we survey some common statistical feature measures.

4.1.1.1 First-order Description Statistics

The digital image can be represented as a two-dimensional array in the computer. The allowed gray-level values of a pixel range from 0 to $2^b - 1$, where b is the number of bits of the image. For most digital images, 8 bits are sufficient and the gray-level values range from 0 to 255. Lower values are attributed to darker pixels, and higher values to brighter pixel. Therefore black is represented by 0 and 255 represents white in an 8-bit image. Figure 4.1 (a) shows a 3-bit image what pixels' gray-level values range from 0 to 7 [32]. Image size is 5×5.

The spatial distribution of gray-level variations can be described by a probability distribution of pixel intensity. It is this histogram which is used to generate a class of texture features. One direct way to characterize the qualities of textures is to use the shape of an image histogram.

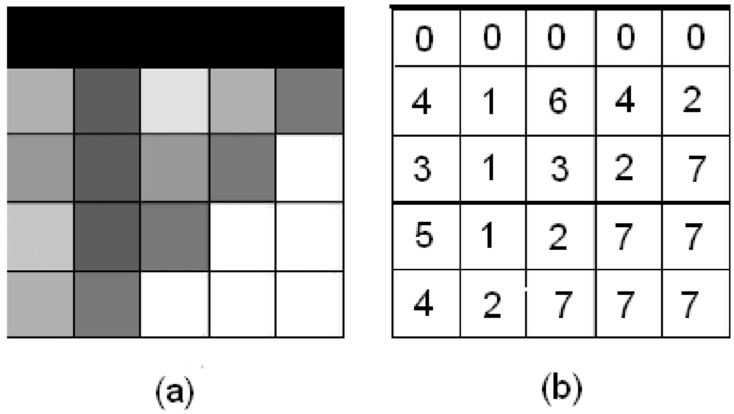

Figure 4.1: An example of a digital image. Graph (a) is a 3-bit image, graph (b) presents gray level values of individual pixels

A histogram with a narrow gray-level distribution indicates a low-contrast image and a bimodal histogram suggests regions of different brightness.

A group of statistical measures which describe the histograms can be calculated from the gray level values of individual pixels in an image, including mean gray level μ of pixels, variance and their standard deviation σ, and signal-to-noise ration ($SNR = \mu/\sigma$). A further characterization of the histogram includes skewness and kurtosis. Skewness is a measure of symmetry. A distribution, or data set, is symmetric if it looks the same to the left and right of the center point. Kurtosis is a measure of whether the data are peaked or flat relative to a normal distribution. That is, data sets with high kurtosis tend to have a distinct peak near the mean and decline rather rapidly. Data sets with low kurtosis tend to have a flat top near the mean rather than a sharp peak.

Some studies using first-order statistic features have been successful in pattern recognition and characterization [12]. However, because the features are generated using the absolute gray level values of the images, the dependence of these features on scanning equipment settings becomes an issue. To get a uniform brightness range, images analyzed should be acquired from the same scanning equipment with the same settings. In addition, a standardized procedure must be used when capturing images; otherwise, any generated feature of the texture images cannot be compared from one image to another.

4.1.1.2 Second-order Description Statistics

Second-order texture measures are mainly based on the joint gray-level histogram of pairs of geometrically related image points. There are two widely used second-order statistics methods: Gray level co-occurrence matrices and gray level difference measures.

Co-occurrence Matrices

Gray level co-occurrence matrices (GLCM) proposed by Haralick [33] have become one of the most well-known and widely used texture measures. Let a two-dimensional image $I(x, y)$, $(x = 1, ..., M, y = 1, ..., N)$, have N_g gray levels. A co-occurrence matrix depicts the joint gray-level histogram of the image (or a region of the image) in the form of a matrix with the dimensions of $N_g \times N_g$. The entries are the joint probability density of pairs of gray levels that occur at pairs of points separated by the displacement vector d.

Suppose $P_d(i, j)$ denotes the cardinality of the set of pairs of points that have gray level values of i and j, for a displacement vector $d = (dx, dy)$.

$$P_d(i, j) = |\{((r, s), (r + dx, s + dy)) : I(r, s) = i, I(r + dx, s + dy) = j\}| \tag{4.1}$$

where$(r, s) \in M \times N$, and $|.|$ is the cardinality of a set. The following example illustrates co-occurrence matrix computations for distance $d = 1$. A 4×5 image with eight gray levels ranging from 1 to 8 is presented in Figure 4.2 (the example is originally from image processing toolbox user's guide for MATLAB. The MathWorks. Incorporated.). Figure 4.2 (a) is the original image, (b) is the gray level co-occurrence matrix representing pairs of gray levels are separated by distance 1 in the 0° direction, that is, the vector $(1, 0)$. To illustrate, the element in row 1, column 2 of the matrix is the total number of times gray level value 2 occurring adjacent on the right side of gray level value 1, that is, $d = (1, 0)$. Figure 4.2 (c) presents a gray level co-occurrence matrix with distance 1 in the direction 45°, that is, $d = (1, 1)$. The calculation of matrices for other six directions $(90°, 135°, 180°, 225°, 270°, 315°, 360°)$ is similar. Note that the matrices so defined are asymmetric since, for example, a co-occurrence of pixels in the 0° direction is recorded separately from the same pair of pixels co-occurring in the 180° direction.

In most cases, we only consider a symmetric matrix where the co-occurrences in opposite directions are combined. Thus, symmetrical GLCM is generated by pooling frequencies of pairs of gray levels occurrences at separation positive or negative distance d pixels. For example, the element in the (0, 0) position of the symmetric matrix is calculated by adding together frequencies of occurrences with distance $d = (1, 0)$ and $d = (-1, 0)$, thus the (0, 0) entry value is 2 rather than 1 in non-symmetric matrix (see Figure 4.3). For both the symmetric and asymmetric matrix, the magnitude of d ensures that the derived texture features will be most sensitive to images exhibiting textural changes over a distance |d| pixels. The selection of the distance |d| is application dependent.

The number of paired occurrences in a given image varies with the magnitude of the vector d because of the edge effects. Consequently, co-occurrence matrices are often normalized to the number of such paired occurrences. Normalization can be achieved by dividing the entries in P_d by the sum of the entry values of the matrix. As a result, the sum of entry values of the normalized

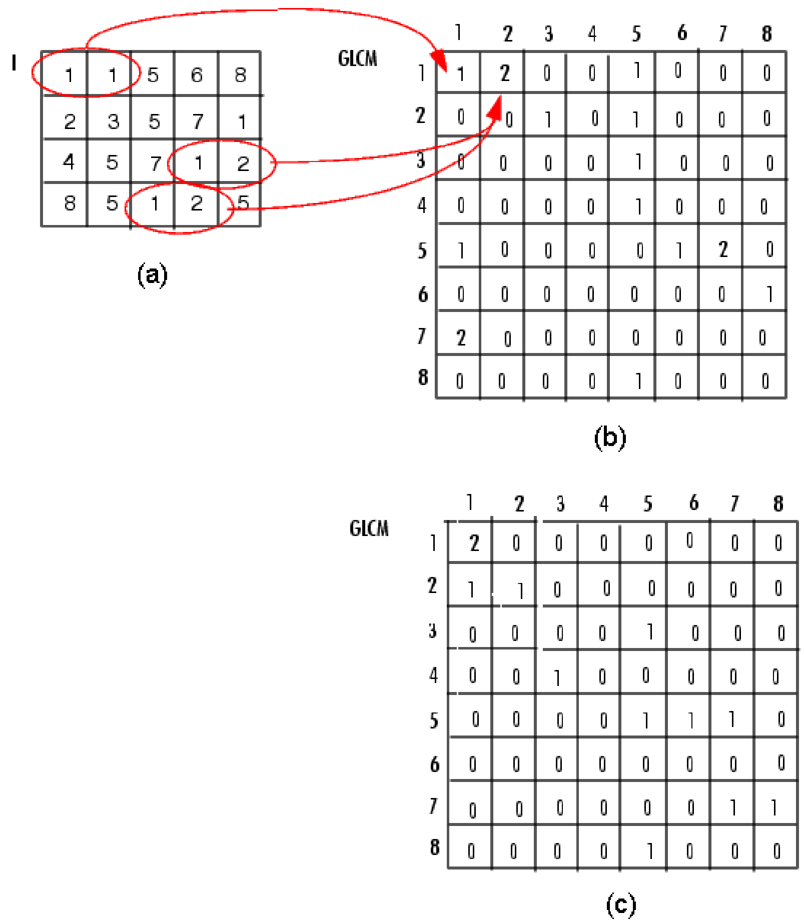

Figure 4.2: Asymmetric gray level co-occurrence matrices. Graph (a) is original image, (b) is gray level co-occurrence matrix in 0-degree direction, (c) is gray level co-occurrence matrix in 45-degree direction (Copyright The MathWorks. Incorporated.)

matrix equals to 1. Haralick et. al., proposed 14 texture features derived from normalized gray level co-occurrence matrices. We discuss some of these features below and the remainder are defined in Appendix A.

Suppose $p_d(i,j)$ is the value of entry (i,j) in a normalized symmetric GLCM matrix and it represents the probability of gray level i occurring at a displacement d from gray level j.

N_g is the number of gray levels in the digital image.

$p_d(i) = \sum_{j=1}^{N_g} p_d(i,j)$, means ith entry in the marginal-probability matrix obtained by summing the ith row of $p_d(i,j)$.

$p_d(j) = \sum_{i=1}^{N_g} p_d(i,j)$, means jth entry in the marginal-probability matrix obtained by summing the jth column of $p_d(i,j)$.

μ_i and μ_j are the means and σ_i and σ_j are the standard deviations of $p_d(i)$ and $p_d(j)$, respectively.

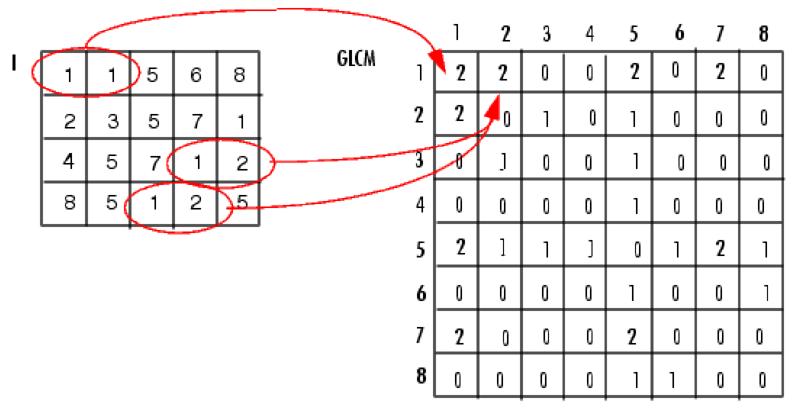

Figure 4.3: Symmetric gray level co-occurrence matrices. Left is the original image, right is gray level co-occurrence matrix in 0-degree direction.

The following equations define some of the features proposed by Haralick et. al.

- Contrast – returns a measure of intensity contrast between a pixel and its neighborhood. Contrast is 0 for a constant image.

$$Contrast = \sum_{n=0}^{N_g-1} n^2 \sum_{|i-j|=n} p_d(i,j) \tag{4.2}$$

- Correlation – measures how correlated a pixel is to its neighborhood. Feature values range from -1 to 1, these extremes indicating perfect negative and positive correlation respectively.

$$Correlation = \frac{\sum_{i=1}^{N_g}\sum_{j=1}^{N_g}(i-\mu_i)(j-\mu_j)p_d(i,j)}{\sigma_i\sigma_j} \tag{4.3}$$

- Homogeneity – measures the similarity of pixels. A diagonal gray level co-occurrence matrix gives a homogeneity of 1.

$$Homogeneity = \sum_{i=1}^{N_g}\sum_{j=1}^{N_g}\frac{p_d(i,j)}{1+|i-j|} \tag{4.4}$$

- Energy – means uniformity, or angular second moment (ASM). The more homogeneous the image, the larger the value. When energy equals to 1, the image is believed to be a constant image.

$$Energy = \sum_{i=1}^{N_g}\sum_{j=1}^{N_g} p_d^2(i,j) \tag{4.5}$$

- Entropy – is a measure of randomness of intensity image.

$$Entropy = -\sum_{i=1}^{N_g}\sum_{j=1}^{N_g} p_d(i,j)\log(p_d(i,j)) \tag{4.6}$$

Energy, entropy, contrast, homogeneity and correlation features are often used among the 14 Haralick texture features to reveal certain properties about the spatial distribution of the texture image. Since real textures usually have so many different dimensions, these texture properties are not independent of each other. For instance, the energy measure generated from gray level co-occurrence matrix is also known as homogeneity and variance is a measure of contrast in images. Therefore when choosing a subset of meaningful features from gray level co-occurrence matrix for a particular application, features do not have to be independent because a subset of fully independent features is usually hard to find. Haralick [33] illustrated the applications of some textural features computed based on co-occurrence matrices. He employed distance 1 co-occurrence matrices to compute angular second moment, contrast, correlation and entropy for categorization tasks for several kinds of images. The identification accuracy was 89% for photomicrographs, 82% for aerial photographic images, and 83% for the satellite images. The classification results indicated that features computed based on the co-occurrence matrices have a general applicability for different kinds of images.

Gray Level Difference Measure

The gray level difference method is similar to the co-occurrence matrices. Texture features are also derived from the probability density functions of gray levels. The difference is that probability densities in the gray level difference method are not directly calculated from the original texture image, but from a subtracted image [34]. For example, let $I(n,m)$ be a original grayscale image. Given a displacement $d = (dx, dy)$, where dx and dy are integers, the subtracted image $\text{diff}(n,m)$ is obtained by

$$\text{diff}(n,m) = |g(n,m) - g(n+dx, m+dy)| \tag{4.7}$$

and probability density function is defined as

$$p(i,d) = P(\text{diff}(n,m) = i). \tag{4.8}$$

This probability density function also can be computed from four principal directions: $0°, 45°, 90°$, and $135°$. Typically the difference density functions are accumulated in the horizontal and vertical direction, or in all four directions in an image, providing rotationally invariant texture measures.

4.1.1.3 Higher-Order Description Statistics

Autocorrelation Measure

Each pixel in a texture image can be characterized by its location properties. We can consider a texture primitive as a contiguous set of pixels described by some properties such as its average intensity, size, position, shape, etc. The autocorrelation function is described by the correlation coefficient that evaluates linear spatial relationships between the texture primitives. It is widely used to assess the amount of regularity in a texture, the size of the texture primitives, as well as coarseness/fineness of the texture in the images. If the texture primitives are large, yielding coarse textures, the autocorrelation function value decreases slowly with increasing distance. If texture primitives are small [35] which gives fine textures, the autocorrelation function decreases rapidly. If the primitives are periodic, the autocorrelation function increases and decreased periodically with distance [35]. In some cases, the autocorrelation function is often utilized as a description of the interrelation between the gray values of neighboring pixels. If the autocorrelation gradually decreases with the distance of the pixels, the pixels become more and more statistically independent. A texture is detected to be anisotropic if gray values of neighboring pixels have a stronger correlation along one direction than along another direction. The texture is isotropic if correlation between gray values of neighboring pixels equal in all directions. If the statistics do not depend on the position of the pixel, the texture is called homogeneous. Scharcanski [36] used such property of autocorrelation function to estimate local spatial anisotropy in texture images.

For a texture image $I(i, j)$, a set of autocorrelation coefficients are given by:

$$C_{II}(p, q) = \frac{MN}{(M-p)(N-q)} \frac{\sum_{i=1}^{M-p} \sum_{j=1}^{N-q} I(i, j) I(i+p, j+q)}{\sum_{i=1}^{M} \sum_{j=1}^{N} I^2(i, j)} \tag{4.9}$$

where p, q are spatial displacements, and M, N are image width and height.

Run length (Primitive length)

The texture description features can also be calculated based on computation of primitive length and gray level. A primitive is a continuous set of maximum number of pixels in the same direction that have the same gray level. A large number of neighboring pixels of the same gray level represents a coarse texture, a small number of neighboring pixels of the same gray level represents a fine texture. Run length texture description features, such as gray-level uniformity, short (long) primitives emphasis, and primitive percentage provide a description vector [35] which can be used as the input vector of a classifier in texture classification tasks.

The run length matrix describes how many times there are r consecutive pixels with the same gray-level value in a given direction. The parameter r ranges from 2 to n, where n depends on the image size and direction of measurement. For example, $n = 5$ in horizontal direction for an image with 5×5. In practice, 4 matrices are computed for $0°, 45°, 90°$, and $135°$ directions. An example of run length matrix is given in Figure 4.4. It is computed from the digital image shown in Figure 4.1.

We often sum up run length matrices in all directions to get a rotationally invariant matrix. Many texture features can then be computed from the run length matrix. We list here five texture description features. Note each one is defined by primitive gray level, length and direction. $B(a, r)$ is the number of primitives of all directions having length r and gray level a, M and N are image

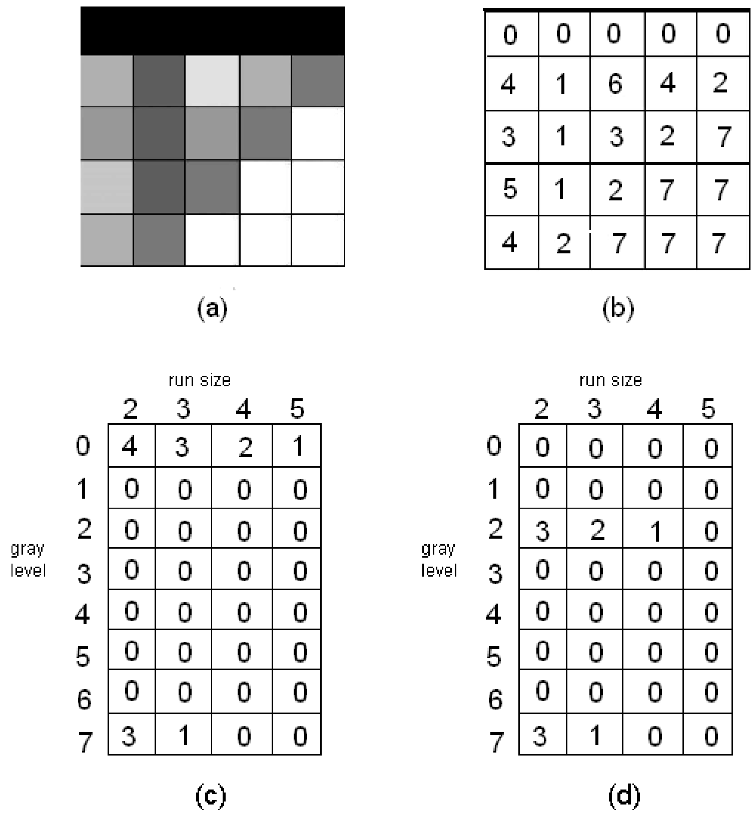

Figure 4.4: Run length matrices. Graph (a) is original greyscale image, (b) presents pixel gray level values, (c) is run length matrix in the horizontal direction, (d) is run length matrix in the 45 degrees direction

dimensions, L is the maximum number of gray levels, N_r is the maximum primitive length in the images, and K is the total number of runs.

- short primitive emphasis:

$$\frac{1}{K}\sum_{a=1}^{L}\sum_{r=1}^{N_r}\frac{B(a,r)}{r^2} \tag{4.10}$$

- long primitive emphasis:

$$\frac{1}{K}\sum_{a=1}^{L}\sum_{r=1}^{N_r}B(a,r)r^2 \tag{4.11}$$

- gray-level uniformity:

$$\frac{1}{K}\sum_{a=1}^{L}\left[\sum_{r=1}^{N_r}B(a,r)\right]^2 \tag{4.12}$$

- primitive length uniformity:

$$\frac{1}{K}\sum_{r=1}^{N_r}\left[\sum_{a=1}^{L}B(a,r)\right]^2 \tag{4.13}$$

- primitive percentage:

$$\frac{K}{\sum_{r=1}^{N_r}\sum_{a=1}^{L} B(a,r)} = \frac{K}{MN} \tag{4.14}$$

$$K = \sum_{a=1}^{L}\sum_{r=1}^{N_r} B(a,r)$$

4.1.1.4 Other Statistical Description Measures

The local extrema measure is another statistical approach used in certain applications. The local extrema measure is based on the study of local extrema of gray level values in images or certain parts of the images. In an image containing various levels of information, a pixel in the image is believed to be a local maximum if it is higher than all the others in a given area centered on this pixel. The order of this local maximum is defined as the radius of this area. Usually, fine textures have a large number of small-sized local extrema, coarse textures have a smaller number of small-sized local extrema [37]. In [38], images were segmented using the information of local extrema, because it was believed that the characterization of texture is provided through the distribution analysis of the local extrema orders.

The texture transform measure represents another approach. Each texture type presented in an image was transformed into a unique gray-level. In [39], local texture orientation was used to transform a texture image into a feature image.

4.1.2 Model-based Methods

Model-based methods were originally developed in the texture synthesis field. They are based on the construction of an image model that can be used not only to describe texture, but also to synthesize it. These models assume that the intensity at each pixel in the texture image depends on the intensities of only the neighboring pixels. The model parameters capture the qualities of texture [40]. Two popular modeling methods, Markov random fields models and fractals, are discussed.

Markov random fields are able to capture the local contextual information in an image by assuming a joint probability for modeling images. It is also called Markov neighbor because the conditional probability of the intensity of a given pixel depends only on the intensities of the pixels in its neighborhood. Markov random fields model have been applied to applications of texture synthesis [41] and texture classification [42]. Markov random fields have several advantages. They emphasize local contextual information, which makes texture classification much easier to achieve. Pixels and groups of pixels are assigned different labels after classifications. This method is convenient for representing some important location attributes in images, such as the location of discontinuities between regions and boundaries in images.

Fractals are very useful in modeling statistical properties such as roughness and self-similarity in images. A deterministic fractal is defined by "self-similarity" as follows [40]. Given a bounded set A in a Euclidean n-space, the set A is said to be self-similar when A is the union of N distinct copies of itself, each of which has been scaled down by a ratio of r [40]. The fractal dimension D is defined as:

$$D = \frac{\log N}{\log 1/r} \tag{4.15}$$

The larger the fractal dimension, the rougher the texture is. Pentland has demonstrated that images of most natural surfaces can be modeled as spatially isotropic fractals [43].

There are many other image models proposed besides Markov random fields models and fractals. Pixel-based models view an image as a collection of pixels, whereas region-based models regard an image as a set of subregions placed according to given rules. Stochastic spatial interaction models treat the intensity process as a stochastic process. The observed intensity function is regarded as the output of a transfer function whose input is a sequence of independent random variables, i.e. the observed intensity is a linear combination of intensities in a specific neighborhood plus an additive noise term. Gibbs random field is a global random field model, where cliques of neighboring pixels are used as the neighborhood system and a probability density function is assigned to the entire image [44]. Detailed discussions of image models are given in [45] and [46].

4.1.3 Syntactic Methods

Some texture definitions regard textures as a regular arrangement of a small number of fixed pixel groupings called primitives. Syntactic texture description models assume that the primitives are located in almost regular relationships, textures are composed of primitive elements and placement rules, and then seek to partition images. A grammar represents a rule for building a texture from primitives. Placement rules represent the spatial relationship between primitives. A number of grammars and different placement rules may usually be used to describe a texture. Grammars suitable for texture description contain chain grammars, graph grammars, tree grammars, and matrix grammars [35].

Syntactic texture description is usually achieved by combining specific primitive description methods. The rules governing the spatial organization of primitives are inferred. Properties of the primitives (e.g., area and average intensity) are then used as texture features. In some applications, the primitives may be extracted by edge detection with a Laplacian-of-Gaussian or difference-of-Gaussian filter [47, 48, 49], others describe the primitives by adaptive region extraction [50], or by mathematical morphology [51]. Once the primitives have been identified, the analysis is completed either by computing statistics of the primitives (e.g. intensity, area, elongation, and orientation) or by describing the placement rule of the elements. Among these methods, image edges are an often used primitive element.

Syntactic texture description can be applied individually, or even combined with other methods. For example, Hong et al. in [52] assumed that edge pixels form a closed contour and primitives were extracted by searching for edge pixels followed with a region growing operation.

4.1.4 Signal Processing Methods

Signal processing methods compute certain features from filtered images. The filters commonly used include spatial domain filters, Fourier domain filters, Gabor filters, wavelet transformation, discrete cosine transformation, ring or wedge filters and so on. Four widely used types of filtering approaches, namely spatial filtering methods, frequency domain analysis, Gabor filters, and discrete wavelet frame transformation methods are introduced in the following sections.

4.1.4.1 Spatial Filtering Methods

Spatial domain filters are similar to operator-based methods and thus could also be classified as a statistical method. A number of texture features, such as edge frequency, coarseness, randomness, directivity, linearity and size and so on can be extracted from the filtered texture images [35]. The Laws' texture measures and edge frequency measures are commonly used and have been successful in many applications. We illustrated them in this thesis as two examples of spatial domain filtering approaches. The Laws' texture features are derived from 5×5 Laws' masks, which are, in turn, derived from three 3×1 vectors. The edge frequency measures are computed from edge pixels which may using operators such as Robert's, Laplacian, Laws', Sobel and Prewitt masks.

4.1.4.2 Laws' Energy Measures

The objective of Laws' measures is the derivation of a set of energy features for each pixel in a texture image, and computation of the energy statistic. These features capture the amount of "energy" contributed to the image by certain structures such as edges, spots, waves, and ripples.

According to the Laws' approach [53], a set of feature masks representing different operations can be derived by convolution. It starts from three basic vectors. They are averaging operator $L3 = (1, 2, 1)$, first difference for edge detection $E3 = (-1, 0, -1)$ and second difference for spots detection $S3 = (-1, 2, -1)$. Convolution of these vectors with themselves and with each other results in the following five vectors;

$$L5 = \begin{pmatrix} 1 & 4 & 6 & 4 & 1 \end{pmatrix} \tag{4.16}$$

$$E5 = \begin{pmatrix} -1 & -2 & 0 & 2 & 1 \end{pmatrix} \tag{4.17}$$

$$S5 = \begin{pmatrix} -1 & 0 & 2 & 0 & -1 \end{pmatrix} \tag{4.18}$$

$$R5 = \begin{pmatrix} 1 & -4 & 6 & -4 & 1 \end{pmatrix} \tag{4.19}$$

$$W5 = \begin{pmatrix} -1 & 2 & 0 & -2 & 1 \end{pmatrix} \tag{4.20}$$

representing weighted averaging, edge detector, spot detector, ripple detector and wave detector respectively. Mutual multiplying of these row vectors and column vectors with themselves and each other results in 25 5×5 Laws' masks, which can extract twenty-five different texture patterns from an image. For example, the mask of $L5^T \times E5$ is sensitive to vertical edges and averaging the difference across the same direction. $E5^T \times L5$ can detect the horizontal edges and also do averaging across the same direction. A listing of all 25 masks is given below.

$$\begin{array}{ccccc} L5L5 & E5L5 & S5L5 & W5L5 & R5L5 \\ L5E5 & E5E5 & S5E5 & W5E5 & R5E5 \\ L5S5 & E5S5 & S5S5 & W5S5 & R5S5 \\ L5W5 & E5W5 & S5W5 & W5W5 & R5W5 \\ L5R5 & E5R5 & S5R5 & W5R5 & R5R5 \end{array} \tag{4.21}$$

For example, $E5L5$ are derived as follows.

$$\begin{pmatrix} -1 \\ -2 \\ 0 \\ 2 \\ 1 \end{pmatrix} \times \begin{pmatrix} 1 & 4 & 6 & 4 & 1 \end{pmatrix} = \begin{pmatrix} -1 & -4 & -6 & -4 & -1 \\ -2 & -8 & -12 & -8 & -2 \\ 0 & 0 & 0 & 0 & 0 \\ 2 & 8 & 12 & 8 & 2 \\ 1 & 4 & 6 & 4 & 1 \end{pmatrix} \tag{4.22}$$

In general, to calculate the energy features from the original images, several steps are needed. First, the original images $I(i, j)$ is filtered with one or more 5×5 convolution masks, which gives a number of feature images $f(i, j)$. Second, a texture energy image $e(i, j)$ is computed from each feature image $f(i, j)$. There are two ways to compute these energy statistics. One is summation of the absolute values or the squared values in a square neighborhood of size $(2L + 1) \times (2L + 1)$ about each feature image pixel (see Equations 4.23 and 4.24).

$$e(i, j) = \sum_{m=-L}^{L} \sum_{n=-L}^{L} |f(i + m, j + n)| \tag{4.23}$$

$$e(i, j) = \sum_{m=-L}^{L} \sum_{n=-L}^{L} \sqrt{f^2(i + m, j + n)} \tag{4.24}$$

Note that all kernels except $L5$ (see equations 4.16, 4.17, 4.18, 4.19, and 4.20) are zero-sum, thus, the mean value of $L5L5$ is also non-zero. In accordance with Laws' suggestions, the $L5L5$ kernel can be used as a normalization image normalizing any energy feature image pixel-by-pixel. For illustration, let $\hat{e}(i, j)$ be the normalized energy statistics for pixel (i, j) and $f_{L5L5}(i, j)$ be the feature image computed from $L5L5$ kernel, then the normalization is shown in equation 4.25 and

4.26. Thus we generate a new set of images, in which each pixel values are equal to the normalized energy at this pixel.

$$\hat{e}(i,j) = \frac{\sum_{m=-L}^{L}\sum_{n=-L}^{L}|f(i+m,j+n)|}{\sum_{m=-L}^{L}\sum_{n=-L}^{L}|f_{L5L5}(i+m,j+n)|} \tag{4.25}$$

$$\hat{e}(i,j) = \frac{\sum_{m=-L}^{L}\sum_{n=-L}^{L}\sqrt{f^2(i+m,j+n)}}{\sum_{m=-L}^{L}\sum_{n=-L}^{L}\sqrt{f_{L5L5}^2(i+m,j+n)}} \tag{4.26}$$

We may also compute a normalized energy statistics directly at each pixel and then add them together. The formulas are given as:

$$\hat{e}(i,j) = \sum_{m=-L}^{L}\sum_{n=-L}^{L}\frac{|f(i+m,j+n)-\mu|}{(2L+1)\times(2L+1)} \tag{4.27}$$

or

$$\hat{e}(i,j) = \sqrt{\sum_{m=-L}^{L}\sum_{n=-L}^{L}\left(\frac{f(i+m,j+n)-\mu}{(2L+1)\times(2L+1)}\right)^2} \tag{4.28}$$

where μ is the average intensity value of feature image, that is,

$$\mu = \frac{\sum_{i=1}^{M}\sum_{j=1}^{N}f(i,j)}{M\times N} \tag{4.29}$$

and M and N are the pixel dimensions of the image.

The final step is optional during calculation of energy features. Because some of Laws' energy measures are directional, they are not rotationally invariant. For example, $L5E5$ is sensitive to vertical edges and $E5L5$ is sensitive to horizontal edges. If we add these two feature images together, we have a single feature sensitive to simple edge magnitude. $L5L5$, $E5E5$, $S5S5$, $R5R5$ and $W5W5$ which are already directionally invariant remain the same. Thus, after the combination, we get 15 features invariant to direction:

$$\begin{array}{ccccc} L5L5 & E5E5 & S5S5 & R5R5 & W5W5 \\ \frac{E5L5+L5E5}{2} & \frac{S5L5+L5S5}{2} & \frac{W5L5+L5W5}{2} & \frac{R5L5+L5R5}{2} & \frac{R5W5+W5R5}{2} \\ \frac{S5E5+E5S5}{2} & \frac{W5E5+E5W5}{2} & \frac{R5E5+E5R5}{2} & \frac{W5S5+S5W5}{2} & \frac{R5S5+S5R5}{2} \end{array} \tag{4.30}$$

Different features compose vectors which are usually used for texture image segmentation tasks. Some other methods similar to Laws' have also been reported [54]. Rather than the "edge-like", "spot-like", "ripple-like" masks used in Laws', a set of vertical, horizontal, diagonal and anti-diagonal masks are applied.

4.1.4.3 Edge Frequency Measures

Edge filters are a good way to capture image textures. Once edges are detected in texture regions, they can be used to define texture descriptors in a variety of ways. For example, one can compute edge density, edge orientation, contrast, fuzziness, or spatial arrangement of edges in the texture image.

The first step in computing edge frequency features is to obtain an edge image. Any edge detection scheme may be used. The Laplacian operator is a very popular edge operator, which has the same properties in all directions and the computed feature is invariant to rotation, however, it often responds doubly to edges that can cause the inaccurate computation of edge frequency. Robert's operator is the oldest and simplest operator whose primary disadvantage is its high sensitivity to noise, because very few pixels are used to compute magnitude. h_1 and h_2 are two Robert's operators in two directions, h is a Laplacian operator.

$$h_1 = \begin{pmatrix} 1 & 0 \\ 0 & -1 \end{pmatrix} h_2 = \begin{pmatrix} 0 & 1 \\ -1 & 0 \end{pmatrix} \tag{4.31}$$

$$h = \begin{pmatrix} 1 & 1 & 1 \\ 1 & -8 & 1 \\ 1 & 1 & 1 \end{pmatrix} \tag{4.32}$$

The basic procedure consists of three stages.

(1) Convolving the texture image with an edge detector. This step produces an edge magnitude and possibly an edge direction image depending on detector used.

(2) Eliminating spurious responses. The output of an edge operator is usually thresholded to decide whether the pixel is a strong edge pixel. If the magnitude of a pixel is greater than a high threshold, the pixel is believed definitely to be edge pixel, if the magnitude of a pixel is less than a low threshold, it is may caused by noise and not an actual edge pixel. Selection of an appropriate threshold can inhibit double edges or multiple responses. However, selection of threshold is not an easy task.

(3) Computing features. Several texture properties may be derived from the edge image using the equations in the following:

(3a) The edge density can be defined as the number of edges, $g(x, y)$, greater than threshold T. The smaller the number, the coarser the texture;

$$EdgeDensity = |\{(x, y) \mid g(x, y) \geq T\}| \tag{4.33}$$

(3b) The edge contrast can be defined by edge magnitude of the edge image. Usually, high contrast textures are defined by large edge magnitudes; and

$$Contrast = average_{x,y}(g(x, y)) \tag{4.34}$$

(3c) Randomness can be described using the entropy of the edge magnitude [33].

$$randomness = -\sum_i \sum_j P(i, j) log_2 P(i, j) \tag{4.35}$$

where $P(i, j)$ denotes the edge magnitude on the position of (i, j) in the image. Usually, random textures are represented by high entropy. Randomness and entropy increase linearly.

The method just discussed has the problem of determining a suitable threshold because it is often impossible to find a global threshold for a whole image. Usually, several different thresholds should be decided and used for a better segmentation result.

Approximating a gradient as a function of distance between pixels is another option rather than computing edge magnitude directly from edge operators. This method has no such disadvantages, is easy to achieve and its result can be modified by increasing or decreasing the range of neighborhood. The algorithm consists of two steps.

(1) Compute the distance-dependent texture description function $g_d(i,j)$ for all pixels of the texture image. It can be computed from the original image I for variable distance d.

$$\begin{aligned} g_d(i,j) = |I(i,j) - I(i+d,j)| + |I(i,j) - I(i-d,j)| + \\ |I(i,j) - I(i,j+d)| + |I(i,j) - I(i,j-d)| \end{aligned} \tag{4.36}$$

(2) Evaluate texture features as average values of gradient in specified distances d:

$$g(d) = \frac{\sum_{i=0}^{i=M} \sum_{j=0}^{j=N} g_d(i,j)}{M * N} \tag{4.37}$$

M and N are pixel dimensions of the image.

Large number of edges are shown in a given area size if texture is fine, whereas smaller number of edges are shown in the same area in coarse texture images. Thus, one can determine the coarseness property of a texture image by evaluation of edge frequency features, which can be computed directly from the gradient $g(d)$. Since the value of $g(d)$ is dependent on a given distance d, the dimensionality of the feature vectors is specified by the number of considered distances d. Usually, micro-edges in the texture images can be detected using small distance operators, while the macro-edges need large-size edge detectors [55]. In the thesis, we varied the distance d from 1 to 7, giving us a total of 7 edge frequency features.

Most spatial domain filtering methods are based on well-known windowing (convolution) operations of images. Since there are many ready-to-use software packages for the operation of convolution, the spatial domain filtering methods are easy to implement and have been widely used. However, there is a problem in using filtering methods, that is, the resulting feature is often not orientation invariant. Extra computation is needed to convert the features into orientationally invariant ones.

4.1.4.4 Other Signal Processing Methods

The frequency analysis of the textured image is achieved by performing filtering in the Fourier domain to obtain feature images. The applications of Fourier domain filtering employ either frequency or orientation selective filters to extract frequency and orientation components as texture features. The number of frequency filters depends on the image size. Six frequency filters centered at 1, 2, 4, 8, 16, 32, and 64 cycles and four orientation filters centered at 0, 45, 90, and 135 had been suggested for an image of size 128 $\times$ 128 to achieve a satisfactory result in [40].

Gabor filters are Gaussian shaped band-pass filters [56]. In [57], texture features extracted from multi-textured images using Gabor filters included linear Gabor features, thresholded Gabor features, Gabor-energy features and so on. A quantitative method based on Fisher's criterion was used to assess the performance of those texture features. The independent component analysis (ICA) is a technique for texture analysis by creating a new data dependent filter bank. The new filters are similar to Gabor filters and enable us to create texture features [58]. This area has received considerable attention during the last decade.

Discrete wavelet frame transformation represents another approach. The use of a pyramid structured wavelet transformation for texture analysis was first suggested by Mallat [59]. In the wavelet transformation, the original image is decomposed into a low-resolution and several detail images. Energy and variance of the detail images are usually extracted for texture analysis. In [60], the local energies from each filtered subband image were used as texture features. The main advantage of wavelet decomposition is that provides a unified framework for multiscale texture analysis.

4.1.5 Hybrid Methods

Hybrid methods, which combine the statistical approaches, model-based approaches, signal processing approaches, and syntactic approaches are extremely successful in some applications of texture analysis. Many applications combine the syntactic and statistical approaches for texture analysis. The technique not only brings many advantages of using the primitive definition, but also decreases or avoids the complexity of grammar inference in syntactic approaches. For example, partly syntactic and partly statistical techniques were used together [35]. The primitives were exactly defined and the spatial relations between primitives were based on probabilities in this study.

Other hybrid approaches combine different categories of texture features to form feature vectors. A study of common filtering techniques for classification was given by Randen and Husoy in [56]. Five categories of features were extracted for texture identification. They were statistical (e.g. co-occurrence), geometrical, syntactic (e.g. regularity features), model-based, and signal processing (e.g. wavelet features). A method based on a space-frequency mode was introduced by Haley and Manjunath in [61]. In this study, a polar form of a 2-D wavelet was developed and used for computing microfeatures. The microfeatures characterized frequency and direction of the texture, which were used later in texture classification.

4.2 Comparison of Feature Extraction Methods

There are a number of general definitions of texture in the computer vision literature. Many texture description measures are proposed according to the different definitions. The different measures capture a texture characteristic such as fineness and coarseness in their own ways. For example, autocorrelation measures are based on finding the linear spatial relationship between primitives. If the primitives are large, it means the texture is coarse and the autocorrelation function decreases slowly with increasing distance. If the primitives are small, texture is fine and the autocorrelation function decreases rapidly. The co-occurrence approach is based on the joint probability distribution of pixels in an image. The run length approach is based on computation of continuous probabilities of the length and the gray-level of primitives in the texture. Thus, coarse textures can be represented by a large number of neighboring and long length of texture primitives.

Real textures usually have many different dimensions, therefore textured properties are not independent of each other. This means that a property of the texture may be described in another way by another method. Moreover, the computational complexity will be greatly increased if too many features are extracted. For efficiency's sake, several selected description methods were applied to the images in our study. In the following section, we compare the five categories of texture description methods based on their main properties and limitations on implementation. Only those which were appropriate for our problem were chosen.

Most textures are defined as contextual properties involving the spatial distributions of gray levels [40]. Therefore, the statistical approaches based on spatial distribution of gray values are generally applicable. In addition, the signal processing methods, most of which are based on filter mask operations, are easy to implement using public software. So we utilized statistical and signal processing approaches in the thesis.

Syntactic methods are not as widely used as statistical methods, because any grammar is a very strict formula and placement rules are based on the idea that primitives have regular spatial relationships. It is impossible to describe textures in reality which are usually irregular, distorted or variant in structure in this way. Moreover, syntactic methods are very sensitive to local noise and structural errors, distortions or variations. To make syntactic description of real textures possible, non-deterministic primitives or stochastic grammars must be defined to substitute for primitives with regular relationships and deterministic transformation rules.

The model-based methods are based on estimation of the model parameters. For example, in texture synthesis problems, model parameters are set to control the type of texture. In texture classification problems, parameters need to be estimated first. However, if the texture structure is unknown, the estimation of the parameters is hard to achieve. Thus, an unfortunate point of model-based methods is that the models are intractable because the issue of estimating model parameters is difficult. A Markov random field model is constructed from a graph consisted of connected nodes. Images are represented by joint probabilities of nodes. One disadvantage of this method is that it has to be utilized along with other methods when the joint distribution of the Markov fields is too complex for computation of means. The estimation of fractal dimension also has problems. Fractals assume that image are self-similar at different scales and the fractal is deterministic. One example of deterministic texture is a checkerboard with strictly ordered array of identical squares. Apparently, most natural textures are not deterministic as described in the definition of fractals, which makes the application of fractals difficult. Furthermore, model-based approaches only capture microtextures well, since the practical considerations limit the order of the model. Model-based approaches also fail with inhomogeneous textures [40].

We note that the statistical methods and signal processing methods are superior to others from the above comparison of properties of each texture description method. A number of other aspects should also be considered when choosing a texture description measure. They are as follows.

(1) Gray scale invariance. We must consider how sensitive the texture feature is to changes in gray scale. In industrial machine vision, for example, where lighting conditions may be unstable, gray scale invariance is especially necessary. Ultrasound images in one data set may be recorded by different ultrasound systems using different techniques and procedures of capturing, which causes the absolute gray levels and contrast of each image may be variable.

(2) Rotational invariance. Does the texture feature vary, if the rotation of the images changes with respect to the viewpoint?

(3) Accuracy with respect to noise. How well does the texture measure tolerate speckle noise in the input ultrasound images? This is particularly important in medical applications where the accuracy of image analysis significantly influences a doctor's decision.

(4) Computational complexity. Medical diagnosis requires a parameter easy to understand and fast to compute. Many texture description measures are computationally intensive that they would be very challenging to implement in clinical practice.

Comparison and evaluation of texture description methods beyond a specific application are not realistic. Some realistic factors except for the four points just mentioned can also influence the performance of the methods, such as the amount of training data in texture classification, the pre-processing of an image, the signal intensity of ultrasound waves, and the resolution level of the system. We also have to consider the availability of the provided background knowledge and limitations of the methods in clinical practice.

Such conclusions can be achieved. First, the model-based approaches are obviously inappropriate to this study because we have no idea about the textures properties of ovulatory and anovulatory follicles at this stage and thus estimation of parameters for a texture model is difficult. Similarly, there is difficulty in defining texture primitives if the syntactic texture description model is used because this model assumes that the primitives are located in almost regular relationships. The spatial distribution of texture primitives in different parts of the ovarian follicles is still unknown. Furthermore, the analysis methods localized in the spatial domain compared with analysis in frequency domain are usually preferred in many medical applications because most features in the spatial domain have specific physical meanings corresponding to physiology. As a result, we chose some of statistical methods and signal processing methods including Laws' energy statistics, co-occurrence matrices, and edge-operator masks, and signal processing methods located in spatial domain.

4.3 Extracting Features from Ultrasound Follicle Images

The statistical methods and the signal processing methods were employed in this thesis according to the conclusions in section 4.2. This section places the emphasis on the co-occurrence matrices, Laws' energy measures and edge frequency measures and takes a brute-force approach to the problem of extracting many candidate texture features from these three groups of measures.

There were eight women monitored in the natural menstrual cycles and seven women developed dominant follicles during the use of OC. For each woman, a series of dominant follicle images were captured over time. Because all the women were monitored using the same equipment and same image acquisition parameters, we did not need to consider the difference errors caused by setting parameters. These images were already pre-processed by the methods presented in Chapter 3 before the extraction of features. The complete pre-processing was composed of selecting follicle walls from the original image, gray level adjustment, and linear scaling the resulting image to gray level values ranging from 0 to 255.

Only rotationally invariant texture features were considered in the work presented in the thesis. As we know, direction of a texture should also be considered when analyzing an anisotropic or directional texture in an image. This greatly increases the complexity of analyses. The workload can be reduced by analyzing or comparing only textures captured from the same viewpoint. Unfortunately, it is very difficult to ensure that images captured have the same rotation and direction in most applications. It is unrealistic, especially in ultrasound examinations, to monitor each patient in the same direction and capture images having the same rotation and movement between each other. Therefore, when dealing with directionally variant features, we must first convert them to invariant features.

4.3.1 Extraction of Co-occurrence Features

We obey the definition of symmetrical co-occurrence matrices when computing the co-occurrence matrix.

The selection of d should be based on the particular images and the objects (i.e., follicles) to be considered because the distance d in the co-occurrence matrix is application dependent. The image pre-processing converted the original ultrasound images into a set of images where only the selected follicle wall areas were shown and the remaining parts were black. It was found that most follicle walls were so thin that the widths were often 1 or 2 pixels in the images. Some parts of the follicle walls were even invisible. This might be caused by imperding ovulation during which a part of the follicle wall becomes thinner and thinner and finally it breaks with the release of the egg. To measure the statistics among the follicle wall pixels, the distance d should be chosen to be equal to or smaller than the width of the follicle wall. If $d > 2$, the co-occurrence matrix is actually measuring the spatial relationship between one foreground pixel and one background pixel. Therefore, any choices of $d > 2$ should be avoided for the accuracy reason. We choose $d = 1$ in computing co-occurrence matrices.

Contrast, correlation, energy and homogeneity are four commonly used co-occurrence features and have been reported successful in many applications ([33], [14]). We also calculated these 4 texture features from co-occurrence matrices for each considered image and explained the significance of these features in terms of the kind of values they took on for images of different textural characteristics. Co-occurrence matrices were first calculated for each pre-processed image for the distance 1 in the horizontal direction (0°), right-diagonal direction (45°), vertical direction (90°), and left-diagonal direction (135°). Rotationally invariant features were obtained by averaging feature values over the four directions. Table 4.1 and 4.2 show two examples of computing features using co-occurrence matrices equations 4.2 to 4.5. The feature values in the 7 day study period were computed from images of two women. One image was recorded in the natural cycle and the other was taken during the use of OC. In the tables, Co denotes contrast feature value, Cr denotes correlation feature value, E denotes energy feature value, and H denotes homogeneity. Features in the last column *Average* are all rotationally invariant.

Table 4.1: Co-occurrence features of the follicle wall from an ovulatory dominant follicle. (Co: contrast, Cr: correlation, E: energy, H: homogeneity. 0 = the day of ovulation.)

day	0°				45°				90°				135°				Average			
	Co	Cr	E	H	Co	Cr	E	H	Co	Cr	E	H	Co	Cr	E	H	Co	Cr	E	H
0	11.8173	-0.1292	0.0528	0.4956	15.5759	-0.253	0.051	0.4078	13.2634	-0.1839	0.0503	0.4591	14.5187	-0.2237	0.05	0.4295	13.793825	-0.19745	0.051025	0.448
-1	10.5964	-0.0976	0.0553	0.5041	13.3671	-0.2027	0.051	0.4304	12.0943	0.1315	0.0522	0.4565	14.0338	-0.2266	0.0516	0.4205	12.5229	-0.16795	0.052525	0.452875
-2	9.8199	-0.0786	0.0563	0.5067	13.234	-0.2225	0.0519	0.4288	11.8126	0.1165	0.0546	0.4744	13.0888	-0.2083	0.0532	0.4354	11.9888255	-0.1681	0.054	0.461325
-3	10.0433	-0.0668	0.0641	0.5332	14.3466	-0.2427	0.0563	0.4069	11.7957	0.1231	0.0562	0.477	12.4931	-0.1695	0.0572	0.4619	12.169675	-0.158275	0.05845	0.46975
-4	8.0567	0.0436	0.0671	0.5775	12.8266	-0.1737	0.0532	0.4483	11.3462	0.0913	0.0553	0.4863	12.084	-0.1355	0.0538	0.4579	11.0783755	-0.096075	0.05735	0.4925
-5	-	-	-	-	-	-	-	-	-	-	-	-	-	-	-	-	-	-	-	-
-6	7.1094	0.1078	0.0824	0.5882	11.2359	-0.1166	0.0661	0.461	9.9005	0.0818	0.0679	0.49	10.7541	-0.0852	0.0664	0.4601	9.749975 5	-0.036075	0.0707	0.499825
-7	5.631	0.1761	0.1148	0.6919	11.6726	-0.1358	0.072	0.4619	10.5909	0.1025	0.0703	0.4906	10.2664	-0.0767	0.0707	0.4904	9.540225	-0.0347	0.08195	0.5337

Table 4.2: Co-occurrence features of the follicle wall from an anovulatory dominant follicle. (Co: contrast, Cr: correlation, E: energy, H: homogeneity. 0 = the day of ovulation.)

day	0°				45°				90°				135°				Average			
	Co	Cr	E	H	Co	Cr	E	H	Co	Cr	E	H	Co	Cr	E	H	Co	Cr	E	H
0	3.5277	0.1804	0.2079	0.8053	5.9939	0.0107	0.138	0.6742	5.0493	0.0668	0.1572	0.7169	5.7106	0.0265	0.1434	0.6868	5.070375	0.0711	0.161625	0.7208
-1	2.9193	0.2703	0.1838	0.8281	4.8095	0.1184	0.1255	0.7166	4.2174	0.1435	0.1409	0.7479	4.9299	0.0921	0.1268	0.7147	4.219025	0.156075	0.14425	0.751825
-2	3.8088	0.1939	0.151	0.8055	6.6152	-0.0028	0.0925	0.6645	5.812	0.035	0.1024	0.6966	6.2982	0.0268	0.0938	0.6719	5.63355	0.063225	0.109925	0.709625
-3	3.9026	0.1511	0.2145	0.7877	6.8024	-0.0518	0.1384	0.6423	6.0937	-0.019	0.1559	0.6788	6.5609	-0.0307	0.147	0.6605	5.8399	0.0124	0.16395	0.692325
-4	-	-	-	-	-	-	-	-	-	-	-	-	-	-	-	-	-	-	-	-
-5	-	-	-	-	-	-	-	-	-	-	-	-	-	-	-	-	-	-	-	-
-6	3.9548	0.2111	0.1281	0.7738	7.1056	0.0227	0.0801	0.6313	6.3031	0.0353	0.0919	0.6721	6.8537	0.0209	0.0817	0.6398	6.0543	0.0725	0.09545	0.67925
-7	4.7675	0.1996	0.1467	0.7561	8.7995	-0.0058	0.0829	0.5573	8.2599	0.0195	0.087	0.5776	8.9448	-0.0149	0.0845	0.5607	7.692925	0.0496	0.100275	0.612925

4.3.2 Extraction of Features using Edge Frequency Measures

Two features were calculated from the edge frequency measures in the thesis. They were the edge density feature and edge contrast feature. We varied the distance d from 1 to 7 when calculating edge density feature, obtaining a total of 7 edge density features for follicle wall images obtained from both ovulatory follicles in women with normal cycles and anovulatory follicles in women using OC. Figure 4.5 and 4.6 describe the average edge density values for ovulatory follicle images and anovulatory follicle images varying d from 1 to 7, respectively. We note that there is no significant difference between the seven distributions for each type of follicles. The width of the follicle wall

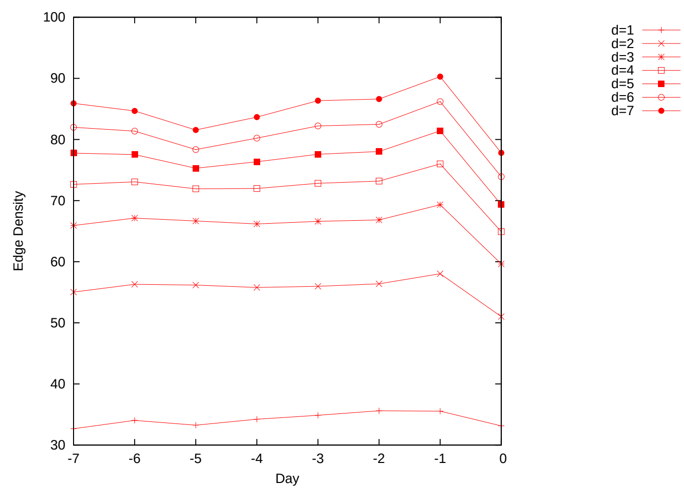

Figure 4.5: Edge density features of ovulatory follicles. The density value increases as the parameter distance d gets bigger, but the difference in the distribution of edge density is not significant when varying d from 1 to 7.

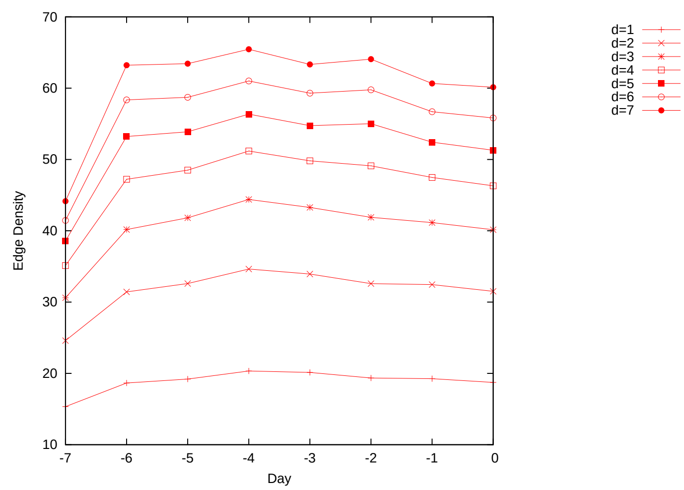

Figure 4.6: Edge density features of anovulatory follicles. The density value increases as the parameter distance d gets bigger, but the difference in the distribution of edge density is not significant when varying d from 1 to 7.

is about two or three pixels according to our problem, therefore we select a distance equal or less than two in order to exclude backgroup pixels in computation. Thus the distance d was chosen to be 1 in this thesis for simplicity. Therefore here the average edge frequencies in the ovarian follicle walls images were measured between the neighbor pixels.

Edge contrast derived from edge frequency measures represents the average value of the edge magnitudes. Edge magnitude was calculated by a 3×3 Laplacian operator in this study. Contrast feature was then computed using image edge magnitude (Equation 4.34).

4.3.3 Extraction of Laws' Energy Features

We computed 4 widely used energy features: $E5L5$, $L5E5$, $E5S5$, and $S5E5$ from the Laws' energy measures [34]. The masks are given in Figure 4.7. Since these four features are variant to rotation, we used the method mentioned in Equation 4.30 to compose two sets of rotation invariant features. The first one derived from $E5L5$ and $L5E5$ energy features was called EL energy and the later one from $E5S5$ and $S5E5$ was called SE energy. Both textuer features EL and ES were computed from the follicle wall images in our data set.

-1	-2	0	2	1
-4	-8	0	8	4
-6	-12	0	12	6
-4	-8	0	8	4
-1	-2	0	2	1

(a) L5 * E5

-1	-4	-6	-4	-1
0	0	0	0	0
2	8	12	8	2
0	0	0	0	0
-1	-4	-6	-4	-1

(b) S5 * E5

-1	0	2	0	-1
-2	0	4	0	-2
0	0	0	0	0
2	0	-4	0	2
1	0	-2	0	1

(c) E5 * S5

-1	-4	-6	-4	-1
-2	-8	-12	-8	-2
0	0	0	0	0
2	8	12	8	2
1	4	6	4	1

(d) E5 * L5

Figure 4.7: Laws' 5×5 center-weighted masks.

4.4 Summary

Five categories of methods for the extraction of texture features were introduced in this chapter. We compared their limitations, complexity of computation, and chose the statistical methods and signal processing methods located in spatial domain. The obtained texture features involved co-occurrence contrast, co-occurrence correlation, co-occurrence energy, co-occurrence homogeneity, edge density, edge contrast, and two Laws' energy features. In the following chapter, we will select from them features which might be used to characterize the follicular development or discriminate ovulatory follicles and anovulatory follicles effectively .

Chapter 5

Feature Selection

It is possible that biological changes of ovarian follicles may be revealed in ultrasound images by the evolution of certain texture properties derived from the images. The properties are represented by extracted texture features. In Chapter 4, five categories of texture description methods were presented. The co-occurrence contrast, co-occurrence correlation, co-occurrence energy, co-occurrence homogeneity, edge density, edge contrast, and two Laws' energy features, were extracted using the statistical approach and signal processing approach. However, not all of the features are independent, and it is computationally expensive to calculate all the texture features for each image in the two data sets (ovulatory follicle images from women in natural cycles and anovulatory follicle images from women using OC). Feature selection is thus an important step in the thesis work for reducing computational workload. Apart from the computational complexity consideration, dimensionality reduction may improve the classification performance. For example, consider a classification problem where the computed texture features are used to compose a feature vector which is then provided as the input of a classifier. Initially performance improves as new feature components are added, but inclusion of further irrelevant feature components may result in an increase in classification error rates. To reduce the computational complexity and at the same time maintain reasonable classification performance, we seek to reduce the dimension of input feature vector by deleting some negligible components.

Eight groups of feature values over time were extracted from each image of the two data sets using the statistical and signal processing texture description methods mentioned in Chapter 4. The aim of this chapter is to identify and select several good discriminators that can classify the two different types of follicles effectively. There are three sections. Principal component analysis for reducing the dimension of feature vectors is briefly presented in Section 5.1, Section 5.2 describes the analyses of different texture features by plotting approach and provides insights into the biological differences between ovulatory and anovulatory follicles. Good discriminantory features are selected in section 5.3 based on the comparison of successful classification rates.

5.1 Principal Component Analysis

Principal Component Analysis (PCA) is a popular approach to reducing the dimension of feature vectors and analyzing data. PCA generates a new set of variables, called principal components. Each principal component is a linear combination of the original variables. Practically, it is common to choose only the first few principal components to reduce computational complexity. This method has been applied to many applications such as face recognition and pattern classification. Chen et al. [62] employed PCA in face recognition and updated the technique to model time-varying statistics, and model the surface reflectance of human faces and reduce illumination variation. Yeung [63] used PCA in clustering gene expression data. In the context of the petroleum exploration field, Posades et al. [64] and Urbancic et al. [65] used principle component analysis to determine the orientation of fault planes from locations of earthquakes and mining induced seismicity. PCA has also been applied to the interpretation of microseismic events resulted by reservoir injections, hydraulic fracture stimulations and other processes [66]. Eigenvectors and eigenvalues were calculated with the maximum eigenvalue corresponding to the fracture orientation as a function of time. In medical image analysis, Haenselmann et al. [67] used a PCA-based method to extract the visual characteristics of texture in order to improve image compression and applied it to texture segmentation. PCA output was regarded as one of the statistical parameters to characterize various brain functions [18]. The brain functions enabled modeling the functional relationships that exist among different regions of the cortex. In Welsh's study of functional relationships of human brain [19], PCA was concerned with explaining the variance-covariance structure of a set of variables. The objectives of PCA were data reduction and interpretation. Welsh's paper also indicated that sometimes the components have a natural physical meaning. For example, when measuring the characteristics of an organism, the first and second component may provide an overall measure of size and shape, respectively.

In principal component analysis, each selected component has no physical meaning. Therefore, PCA method is not employed in the work presented in this thesis. Otherwise the original texture features which should reveal different characteristics or attributes of ovarian follicles will be transformed into a set of new variables which have no longer physical meanings. PCA also requires that the complete components of a feature vector be given for computation of linear combinations, which is actually a weakness of this method because it is difficult to obtain the complete components in most practical applications. Therefore, another consideration for not using the PCA is that it does not reduce the number of original features that have to be extracted. If apply PCA to our thesis study, a complete set of original features also has to be extracted. However, it is difficult because the types and the amount of texture features which characterize the follicular development or are influenced by the use of OC are still not decided.

5.2 Feature Characterization by Plotting Approach

This section tries to provide a basis for understanding how texture features vary over time and identify differences between the two classes of follicles by comparing the feature plots. The basic procedure of plotting in this thesis was as follows. Suppose a set of feature values over time $(v_0, v_1, ..., v_p)$, among which v_0 indicates the value of a feature that is calculated either from images on the day of ovulation in the natural cycles or from images on the day where the E2 peak value appears in the OC cycles, and v_p denotes the feature value on the pth day before the day on which v_0 is computed. By plotting these values of the feature in a time sequence, the graph provides us an approximate trends of the data set. In a two dimensional graph, the horizontal axis normally denotes cycle day and the vertical axis denotes the feature value. Feature value on every day was measured and plotted for women who were monitored every day during the cycle. For women who were monitored every two or three days, only feature values on these inspected days were calculated and plotted. Curves between days were obtained by linear interpolation.

The plotting approach is easy to implement and usually provides useful insights. For example, the variation of a texture feature may indicate biological changes in hormonal levels (i.e., E2 levels) or follicle sizes within the 7 day study period. Sometimes differences between the two groups of follicles may be visually identified from the plots. Another advantage of the plotting approach is that it is not only a visual tool for analysis of the features, but also is a reliable means of omitting irrelevant features. Features which remain approximately constant regardless of the cycle days, or only change minimally will not be used as satisfactory discriminators because they can not provide enough information about physiologic changes in ovarian follicles. In such cases, the plotting approach actually performs selection of the most relevant subset comparable to the full set of features in data set. Features which are not in the subset may not be important or relevant to our problem. This method will work very well if prior knowledge is available.

5.2.1 Co-occurrence Energy Feature

The energy feature, also called angular second moment, is a measure of homogeneity of the image. For illustration, we used images from two randomly chosen women, one of which was from the natural data set and the other from the OC data set. Feature values from follicle wall images during the study period were calculated. For ovulatory follicles, the study period was from the 7th day before ovulation to the day of ovulation. For the anovulatory follicles, the study period was from the 7th day before the appearance of E2 peak to the day following the sudden drop of E2 after reaching its peak. Figure 5.1(a) shows the variations of energy features in four directions (0°, 45°, 90°, and 135°) for the follicle wall images taken from the natural cycle data set and (b) shows the feature variations from the OC cycle data set. In both Figure 5.1 (a) and (b), larger energy feature values were observed in the direction of 0° and comparatively smaller feature values were computed from the other three directions. It demonstrated that texture in the direction of 0° is more constant which may caused by the ultrasound wave transfers from the direction of 0°. Figure 5.1 describes

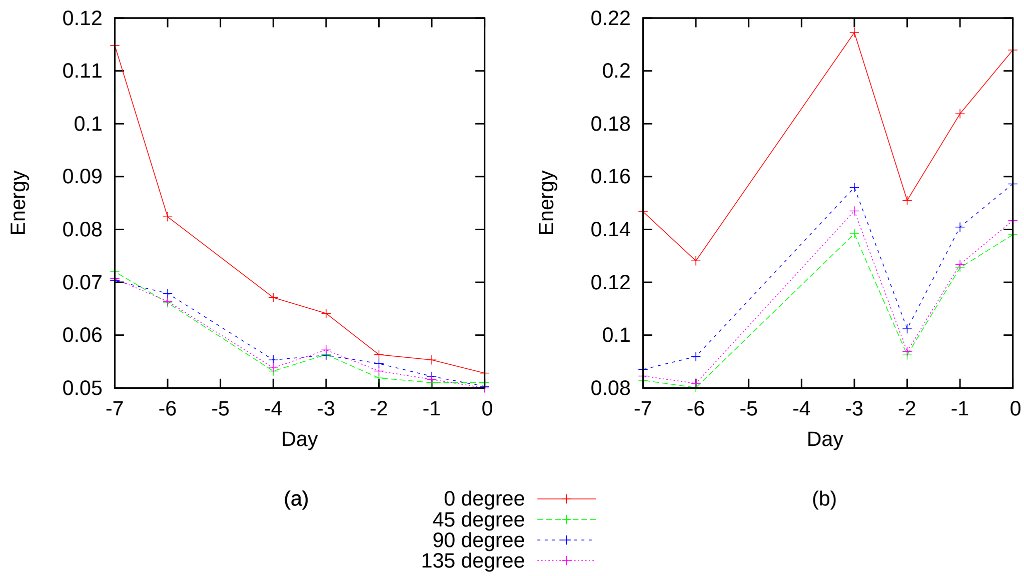

Figure 5.1: Co-occurrence energy features in four directions. Graph (a) was from follicle wall images of a woman in the natural cycle group, (b) was from images of a woman in the OC cycle group.

textures in four different directions (0°, 45°, 90° and 135°). To obtain rotationally invariant gray level co-occurrence energy feature, features should be averaged over all directions. The rotation invariant feature values were computed in the last column of Tables 4.1 and 4.2. Figure 5.2 reports the evolution of co-occurrence energy in the follicle wall regions over time. There are 7 groups of anovulatory follicle wall images and 8 groups of ovulatory follicle wall images, the x-axis denotes the day of a cycle. Looking at how the values vary, we found that the follicle wall images (eight were from the natural cycles and seven were from the OC cycles) could be separated into two categories in the feature space if choosing an appropriate curved discrimination function. We also noted that the values for the follicle wall images from one group of women was consistently greater than the values from the other group of women with a very low p-value (p ¡ 0.0001). Interestingly, the group of curves with consistently larger values corresponded with OC group, whereas the curves with smaller values were all from the natural cycle data set. This indicates that energy feature can be used effectively to discriminate the two categories of follicle walls.

5.2.2 Co-occurrence Homogeneity Feature

The homogeneity feature is a measure of gray-tone transition in the image. In a homogeneous image there are few gray-tone transitions, and the feature value is typically large. Hence, the more homogeneous the texture, the larger the homogeneity value. Homogeneity for ovulatory follicle wall

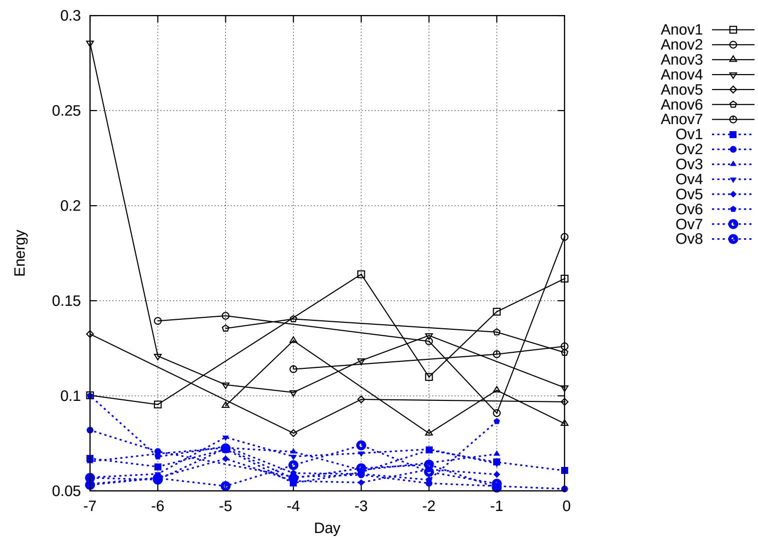

Figure 5.2: Co-occurrence energy features. Anov1 to Anov7 were from the natural cycle group, Ov1 to Ov8 were from the OC cycle group.

images is presented in Figure 5.3 (a). Homogeneity for follicle wall images from the OC data set are drawn in Figure 5.3 (b). Homogeneity values were apparently higher in the horizontal direction

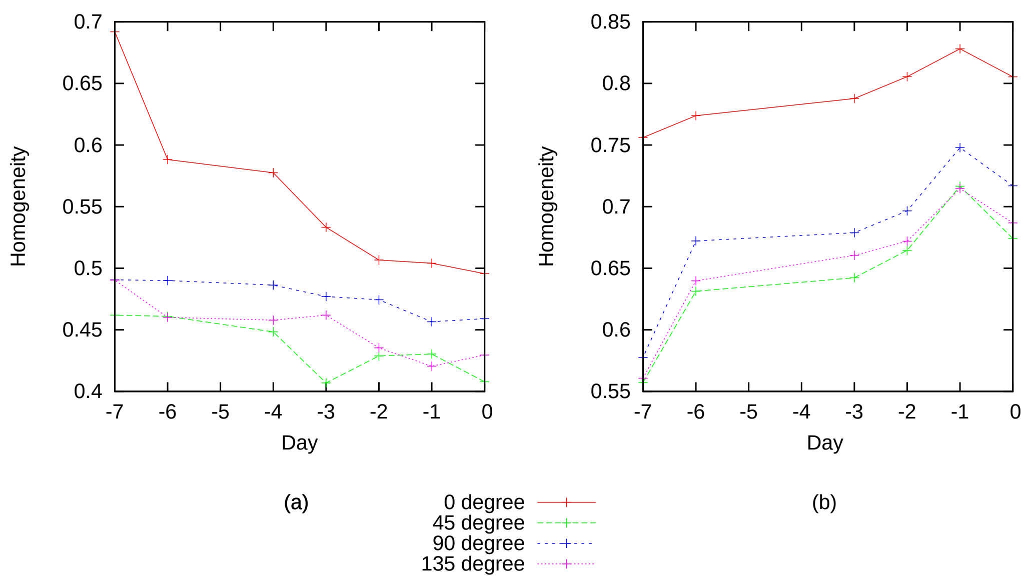

Figure 5.3: Co-occurrence homogeneity features in four directions. Graph (a) was from images of a woman in the natural cycle group, (b) was from images of a woman in the OC cycle group.

(0°) for both categories of follicle wall images.

Rotationally invariant homogeneity feature was obtained after averaging feature values over the direction of 0°, 45°, 90°, and 135°. The evolutions of homogeneity features over time are shown in the Figure 5.4. Follicle wall images in the OC data set were found to have consistently higher homogeneity than images in the natural cycle data set with a p-value lower than 0.0001. Therefore,

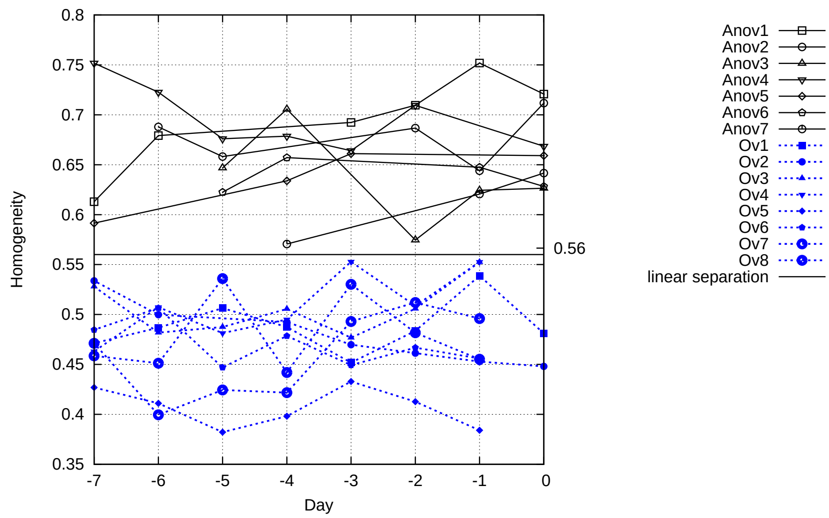

Figure 5.4: Co-occurrence homogeneity features. Anov1 to Anov7 were from the natural cycle group, Ov1 to Ov8 were from the OC cycle group.

a discriminator function can also be found to separate the two categories of follicle images.

5.2.3 Co-occurrence Contrast Feature

The contrast feature is a measure of contrast or the amount of local variations present in an image. Feature values from both an ovulatory follicle and an anovulatory follicle were calculated in four directions similar to the above procedures of analysis (see Figure 5.5). The consistently lower contrast value for the direction of 0° compared to those in the other three directions in both

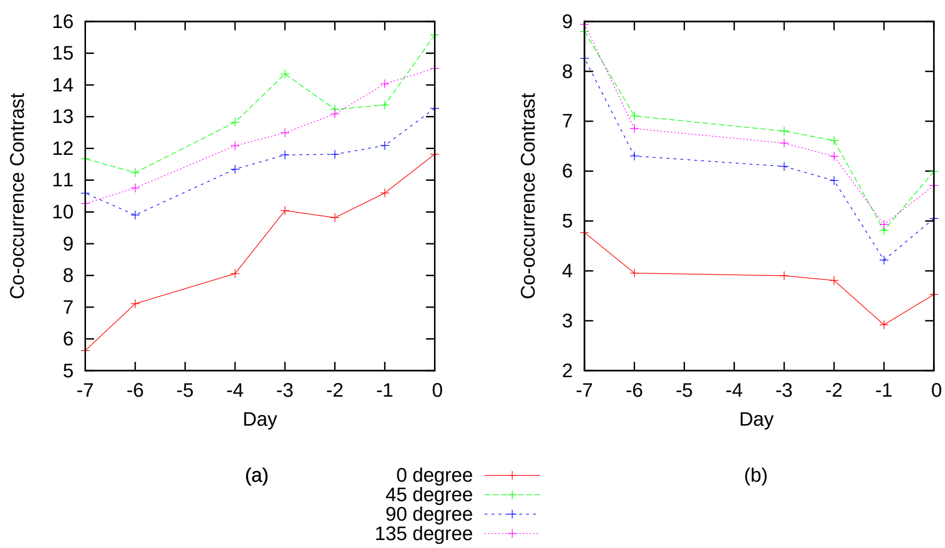

Figure 5.5: Co-occurrence contrast features in four directions. Graph (a) was from follicle images of a woman in the natural cycle group, (b) was from images of a woman in the OC cycle group.

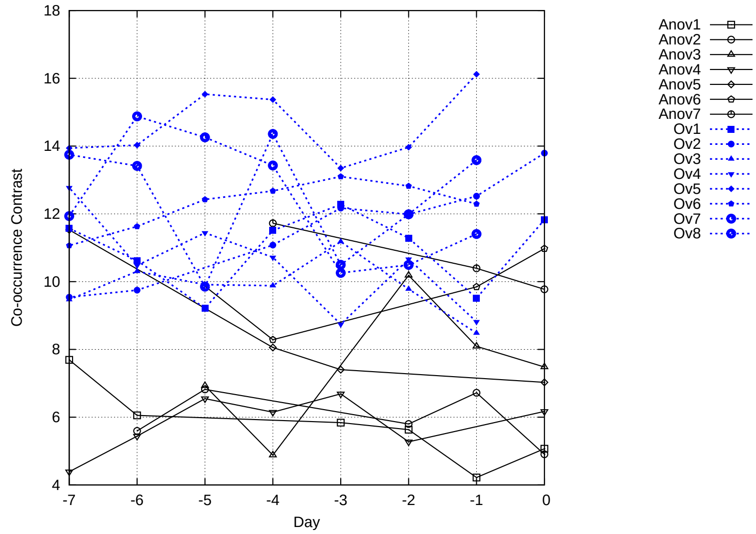

Figure 5.6: Co-occurrence contrast features. Anov1 to Anov7 were from the natural cycle group, Ov1 to Ov8 were from the OC cycle group.

Figure 5.5 (a) and (b) means a smaller amount of local variation present in the direction of 0° in the texture images.

Figure 5.6 describes the variations of rotationally invariant contrast feature for images in the two image data sets. The feature values can be seen to oscillate, exhibiting no obvious patterns for the two categories of images. It is thus impossible to define a threshold that will isolate one group of women from the other on any given day. Contrast is not an effective discriminator for classification of the various follicle walls.

5.2.4 Co-occurrence Correlation Feature

The correlation feature is a measure of gray-tone linear dependency in the image. The correlation feature was consistently higher in the horizontal direction (0°) for both images in different categories of cycles (see Figure 5.7). Since correlation and contrast are correlated textural properties, knowing the variation of one feature can be used to deduce the corresponding change of the other. Therefore, we can also obtain the same conclusion by observing that contrast feature for 0° is lower than that in other directions.

It is obvious that no threshold can be defined to separate the two groups of images apart in the feature space of co-occurrence correlation (shown in Figure 5.8). Therefore, correlation is not a good discriminator for classification of the two groups of follicles.

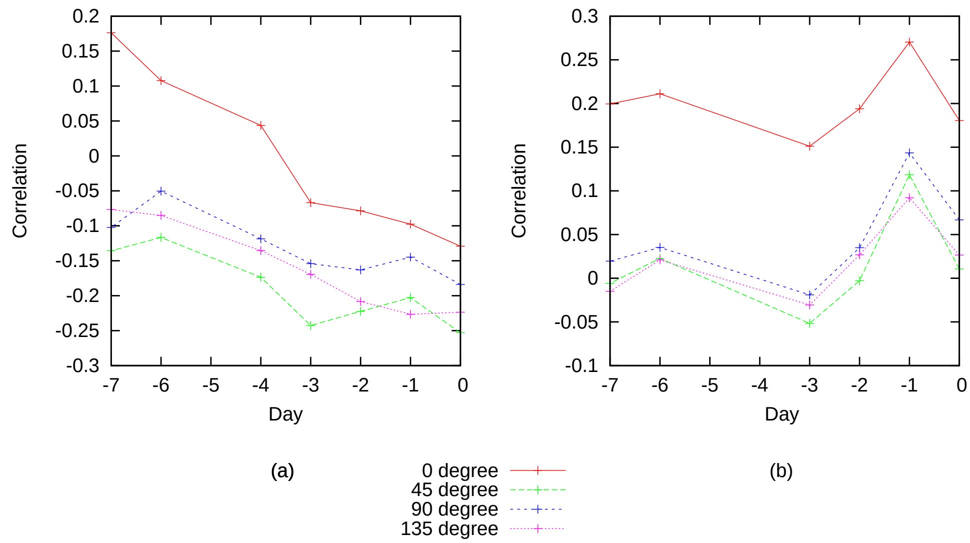

Figure 5.7: Co-occurrence correlation features in four directions. Graph (a) was from follicle images of a woman in the natural cycle group, (b) was from images of a woman in the OC cycle group

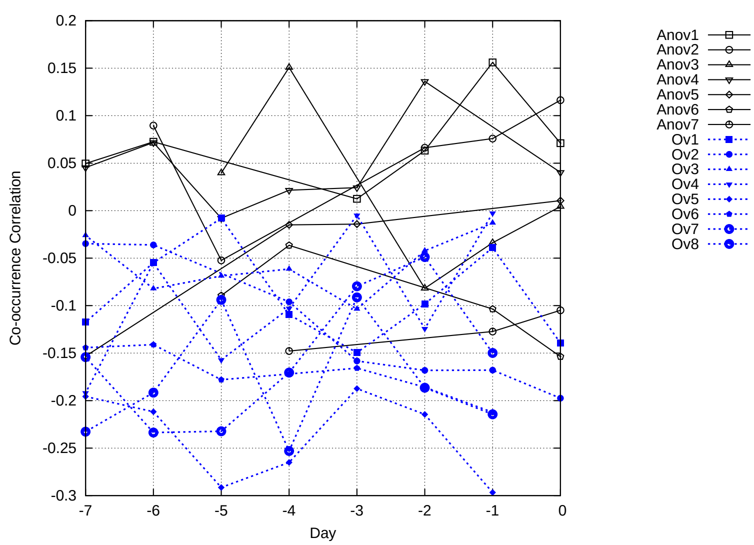

Figure 5.8: Co-occurrence correlation features. Anov1 to Anov7 were from the natural cycle group, Ov1 to Ov8 were from the OC cycle group.

5.2.5 Edge Density Feature

Edge frequency features on the last 7 days before the appearance of E2 peak values or the day of ovulation are plotted in Figure 5.9. We find that the two categories of images are almost separated into two groups in the feature space. The feature values of the follicle wall images from the natural menstrual cycles were found to be consistently higher than the values obtained from the OC follicles with a low p-value (p ¡ 0.0001). Therefore, edge density feature can be taken as an effective discriminator for the classification of two classes of follicles. We observed that

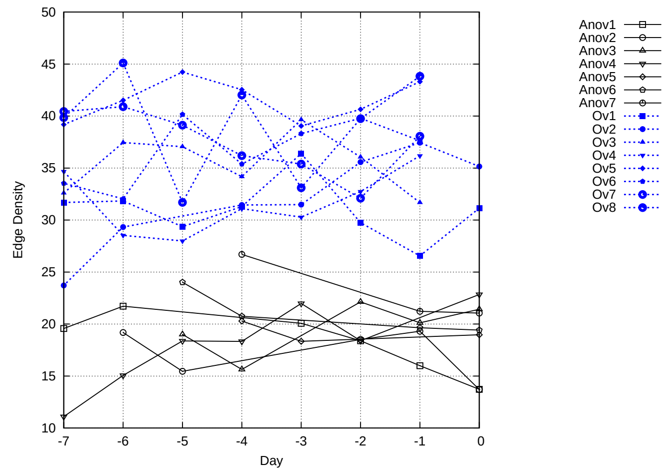

Figure 5.9: Edge frequency features of follicle wall images. Anov1 to Anov7 were from the natural cycle group, Ov1 to Ov8 were from the OC cycle group.

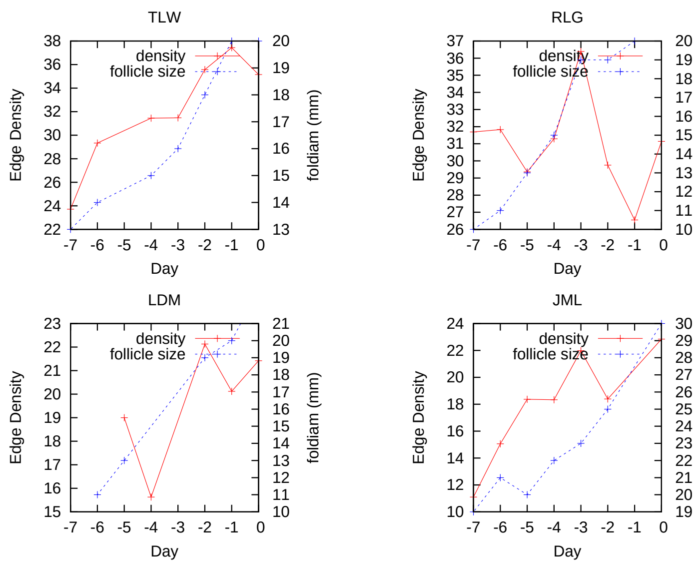

Figure 5.10: Edge density feature and follicle size. The above two plots are from the natural cycle group; the bottom two are from the OC group

all the follicle wall images from the OC data set have a relatively small range of variation in the edge density feature values, whereas feature values computed from images in the natural cycles are subject to larger range of variation or deviation. This variation in the natural cycles is believed to be caused by the generation of a new texture over time. In contrast, the small range of variation in coarseness or smoothness in the OC data set indicates the biological status of the ovarian follicle is relatively stable influenced by the use of OC. This phenomenon is expected due to the effects of exogenous stenosis on the follicles as they develop.

We randomly chose four women from both data sets to illustrate how edge density varied over time with follicle diameter for both two data sets. TLW and RLG were two women from the natural cycle group and LDM and JML were from the OC cycle group. Edge density values when the distance $d = 1$ were calculated for each women. In Figure 5.10, the left y-axis indicates the

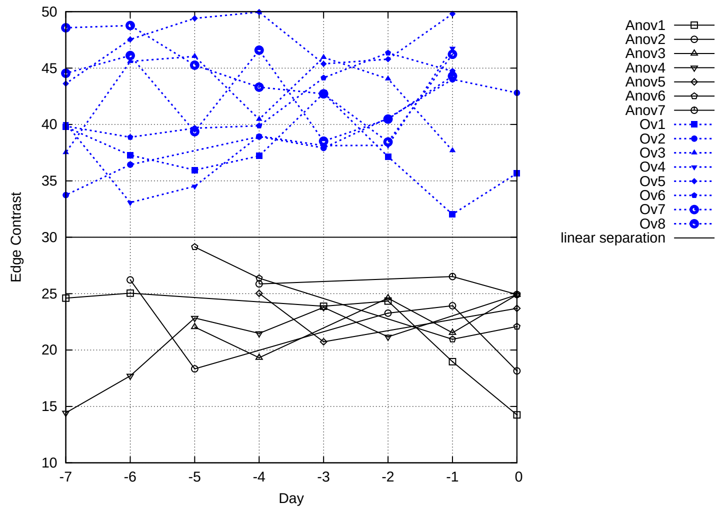

Figure 5.11: Edge contrast features of follicle wall images. Anov1 to Anov7 were from the natural cycle group, Ov1 to Ov8 were from the OC cycle group.

value of edge density, and the right y-axis indicates diameter of the dominant follicle. The edge density feature experiences a local maximum of the feature value on around the 3rd day before ovulation as follicle size increases over time, except for one follicle image from woman who seems to have the highest value on the 2nd day before ovulation. The appearance of maximum edge density might be correlated with certain physiological changes around the 3rd day prior to ovulation or peak estroidol for both ovulatory and anovulatory follicles, respectively.

5.2.6 Edge Contrast Feature

The edge contrast values of the follicle wall images for each inspected woman are plotted in Figure 5.11. The evolution of the edge contrast feature is found corresponding to that of the edge density feature as expected. Feature values from the OC cycle group are smaller than those from the natural cycle group (p ¡ 0.0001). Ovulatory follicles and anovulatory follicles can also be separated by a discriminator function on the feature value. Therefore, edge contrast is good texture feature for characterizing the two different types of follicles. Edge contrast derived from the edge frequency measures is often approximated by co-occurrence contrast derived from co-occurrence matrix because they are not independent with each other. This can be viewed in our results where their evolutions over time were found to be similar.

5.2.7 Laws' Energy Features

Two rotationally invariant energy statistics, $E5S5/S5E5$, and $E5L5/L5E5$, were computed from Laws' measures in the previous chapter. The two texture features are plotted and the variations of these features over time are shown in Figure 5.12 and 5.13. Looking at the figures, it is hard to define a threshold line to separate the two categories of follicle images into two groups for both the

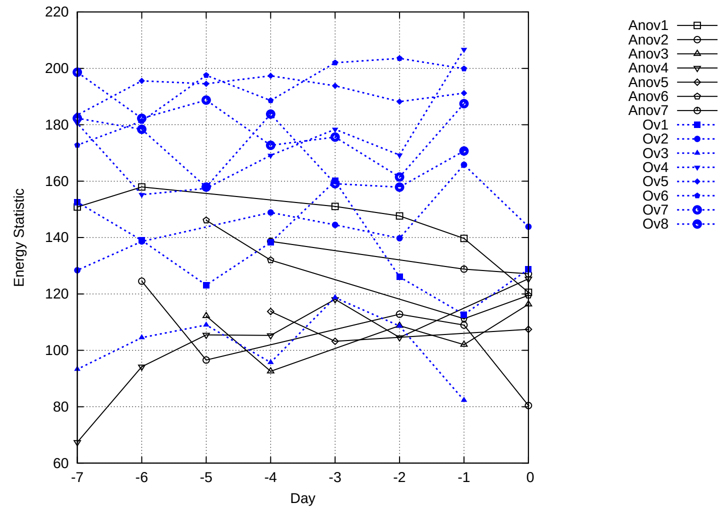

Figure 5.12: Laws' E5S5 energy features of follicle walls images. Anov1 to Anov7 were from the natural cycle group, Ov1 to Ov8 were from the OC cycle group.

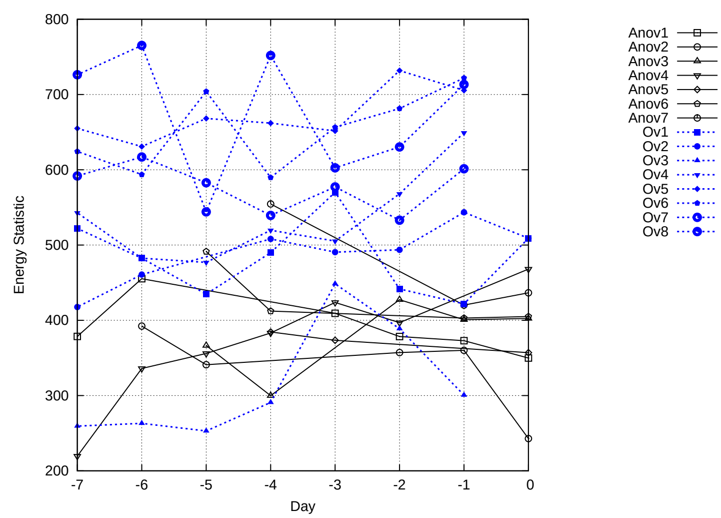

Figure 5.13: Laws' E5L5 energy features of follicle walls images. Anov1 to Anov7 were from the natural cycle group, Ov1 to Ov8 were from the OC cycle group.

energy statistics. Therefore they are not appropriate features.

5.3 Selection of Discriminator Features

The plotting approach discussed above visually depicts feature characterizations over time. We want to further compare quantitatively their performances in classification of the two groups of ovarian follicles, in other words, we want to know the successful rate or misclassification rate using a single texture feature as an input to a classifier. There are only small amount of samples available currently (7 samples in the OC data set and 8 samples in the ovulatory data set). We randomly chose 3 samples from each data set as training data. The remaining 9 were used as testing samples. These samples can be regarded as a group of vectors of correlated random variables. For example, n random vectors v_1, v_2, ..., v_n, each of dimension p. The vectors arise from taking measurements on p days for each of n texture features. Thus both p and n equal to 8.

To classify the two groups of samples, we simply assumed the p-dimensional feature vector of random variables obeyed a normal distribution. Therefore, the main idea was to fit a multivariate normal density to each data set, such that the difference of the means in the two groups was maximum and each observation in the sample data was assigned to its nearest group [68]. The classifier is accomplished using MATLAB functions (e.g. classify()) from MATLAB Statistics Toolbox. The correct classification rate is shown in Table 5.1. Edge density, edge contrast, co-occurrence homo-

Table 5.1: Single-feature correct classification rate of ovulatory and anovulatory follicles

Feature	Correct Classification Rate
Edge Density	100%
Edge Contrast	100%
Co-occurrence Energy	100%
Co-occurrence Homogeneity	100%
Co-occurrence Contrast	66.7%
Co-occurrence Correlation	44.4%
Laws' E5S5 Energy Statistic	77.8%
Laws' E5L5 Energy Statistic	77.8%

geneity and energy were found to be the best discriminators for the given data set. All of them may be used to classify the two groups of follicles correctly. The only difference between them was that edge contrast and homogeneity could be used to adequately separate the two group of follicles by a straight line (see Figure 5.11 and 5.4), whereas edge density and energy feature had to use a curved discriminant function for adequate separation. The two Laws' energy statistics had the same correct classification rate for this particular study, both were better than the co-occurrence contrast. Correlation appeared to be the most ineffective discriminator in our study.

5.4 Summary

Feature values for co-occurrence energy and co-occurrence homogeneity computed from the follicle wall images in the OC data set had consistently higher values than those computed from images in natural cycles during the study period. Values for the edge density and edge contrast feature computed from follicle walls in natural cycles were comparatively higher. Higher homogeneity and energy and lower edge density indicated that the walls of dominant follicles during OC use were comparatively coarser. The results may be attributed to cellular debris during the regression of the anovulatory follicle. The lower homogeneity values detected in ovulatory follicle wall images were attributed to the biological changes during follicular growth or the generation of new cell layers. In contrast, walls of healthy and ovulatory follicles in normal cycles usually have fine textures.

Chapter 6

Statistical Analysis of Texture Features

Two tasks were achieved in the previous chapters. A number of texture features were extracted from ovarian follicle ultrasound images of women in natural cycles and women using OC. Texture features which were deemed to be suitable for characterization of the ovarian follicular development were selected. However, the specific trends of the features during follicular development and the quantitative differences between the feature values were not answered. Accordingly, two main objectives are addressed in this chapter. One is to characterize the distribution of feature values and compare ovulatory follicles and anovulatory follicles statistically. The second objective is to analyze trends of the selected texture features over time. We are particularly interested in testing whether a texture feature has an increasing trend, decreasing trend, cyclical fluctuations, irregular variations, and whether or not a texture feature has a turning point which might be used to identify a physiologically important stage of follicular development. The analysis of texture features is divided into two steps: Measurement of differences between the two data sets and trend analyses.

The main approaches to measurement of difference and trend analysis are using various statistical techniques such as graph, charts, box analysis, mean, standard deviation, and statistical tests.

6.1 Measurement of Mean Group Differences

In the previous chapter, we focussed on several texture features that could be used as discriminators in the classification of two types of ovarian follicles. The texture features included energy, homogeneity, edge density and edge contrast. The first two features were derived from the co-occurrence matrices and the last two were derived from the edge frequency measures. Since the ultrasound images were captured over time, the values of the texture features can be taken as time series data on successive days of their development. We categorized the derived texture features into two groups: features calculated from follicle images of women with natural cycles and those calculated from images of women using OC. We aimed to compare the physiological differences between the two groups. Two basic statistical parameters of populations, the mean feature value and the standard deviation, were computed. The mean and the standard deviation were regarded

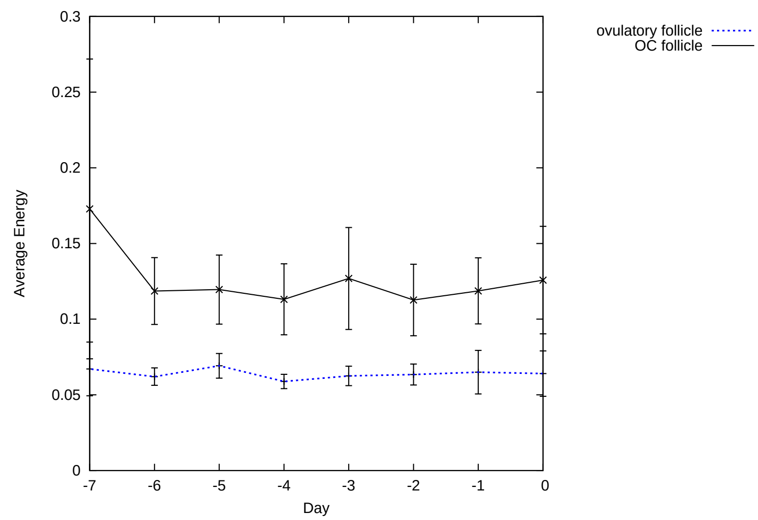

Figure 6.1: Average values of co-occurrence energy and their standard deviations. 0 = the day of ovulation for ovulatory follicles and day after decline of E2 peak for anovulatory follicles

as measures of variability for the feature trend during the 7 day study period.

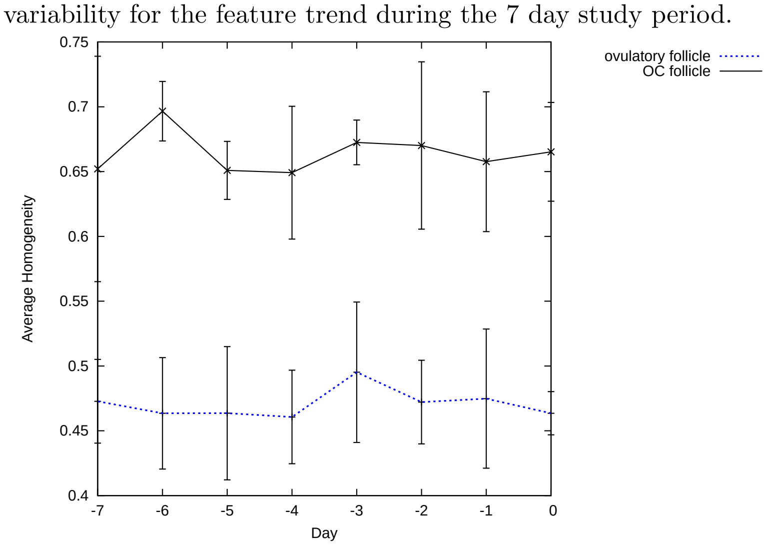

Figure 6.2: Average values of co-occurrence homogeneity and their standard deviations. 0 = the day of ovulation for ovulatory follicles and day after decline of E2 peak for anovulatory follicles

The mean values of energy, homogeneity, and their standard deviation for both groups are shown in Figure 6.1 and 6.2. The dotted curves describe the variation of feature values in ovulatory follicles and the solid curves represent the features in anovulatory follicles during the use of OC. The mean values of energy and homogeneity for follicle walls during the use of OC were consistently higher than those for follicle walls obtained from women in natural cycles, which demonstrates that texture in ovulatory follicle walls was not as homogeneous as anovulatory follicle walls due to the growth of follicles or generation of new textures.

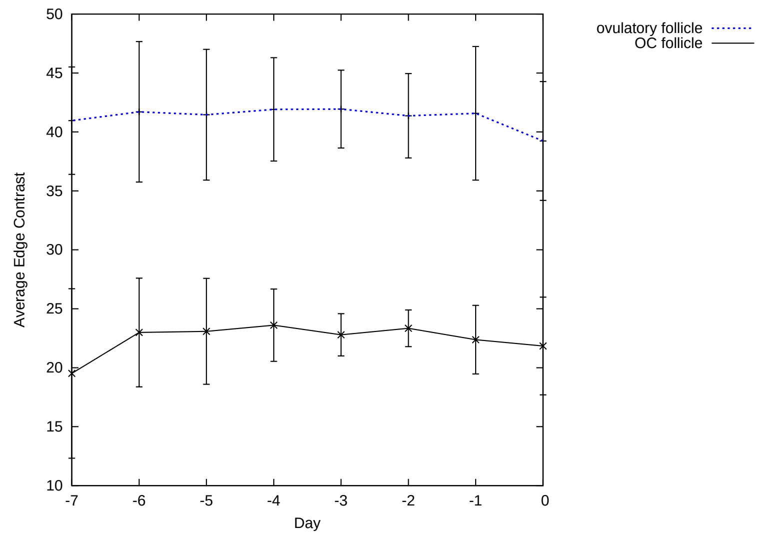

Figure 6.3: Average values of edge contrast and their standard deviations. 0 = the day of ovulation for ovulatory follicles and day after decline of E2 peak for anovulatory follicles

Standard deviation describes how tightly a set of values is clustered around the mean value of those same values. Standard deviation is a measure of dispersal, or variation, in a group of numbers. Higher standard deviation is often interpreted as higher volatility. In comparison, lower standard deviation values would likely be an indicator of stability. The most consistent values will usually be the set of numbers with the lowest standard deviation. For example, we noted that the energy feature had a relatively lower standard deviation for ovulatory follicles than for OC follicles, which told that energy calculated from images of women in natural cycles were tightly centered around the mean values (Figure 6.1). Additionally, comparatively large standard deviation values were observed in the OC data curve. This result was attributed to the smaller number of images on each. For example, there were only two images available from the OC data set on the last inspected day. Also, on the 6th day before day 0, there were only 3 images captured.

The edge contrast feature (Figure 6.3) and homogeneity feature are actually dependent and either one can be approximated by the other one. The relationship between them is that the more homogeneous the texture, the lower the contrast value.

The mean values of edge density feature in both data sets and their standard deviation are shown (Figure 6.4), assuming the distance $d = 1$. Edge density feature values calculated from ovulatory follicle images of women in natural cycles were also consistently higher than that calculated from anovulatory follicle images. We obtained the result that there are more edges on average in follicle wall images in natural cycles. In other words, normal, ovulatory follicles have finer textures in follicle walls, whereas follicles which develop in women taking OC usually have coarser textures.

Obvious differences in feature values between the two categories of follicles were detected in the present study. The result was obtained using our current data set, that is, images from 15 women. However, quantitative difference between the two groups will vary with more and more

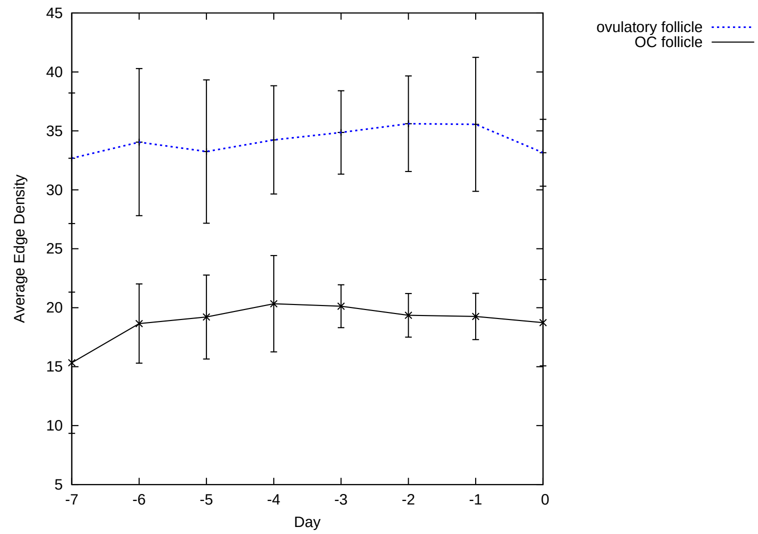

Figure 6.4: Average values of edge density (d=1) and their standard deviations. 0 = the day of ovulation for ovulatory follicles and day after decline of E2 peak for anovulatory follicles

sample images added. True difference between the two groups of follicle images thus has to be measured statistically. One direct way for comparing two groups statistically is to compute the mean difference between their feature values. In the following, some statistical techniques are used for estimation of the group mean difference.

The basic procedure for measuring mean differences between two groups of data is as follows. Suppose that the values of a certain texture feature recorded over time in the natural cycles are independent of those in the OC cycles. The mean difference is a measurement of dissimilarity of two groups of data. For illustration, A denotes one group of mean feature values $f_1, f_2, ..., f_N$, computed from ovulatory follicles in women with natural cycles, f_N means the value of a texture feature which is calculated from an image captured on the Nth day in a cycle. B denotes a group of values $f_1^{'}, f_2^{'}, ..., f_N^{'}$ of the same texture feature calculated from the OC cycle. The number of recorded features in A and B is equal. Subtracting in the same order (in this case, A value minus B values), a set of difference values D, $d_1, d_2, ..., d_N$, are obtained.

$$d_i = f_i - f_i^{'}, (i = 1, 2, ..., N) \tag{6.1}$$

From the sequence of D, the mean difference is estimated as:

$$\overline{D} = \sum_{i=1}^{N} d_i/N. \tag{6.2}$$

The variance of the mean difference is:

$$S_D = \frac{1}{N} \sum_{i=1}^{N} (d_i - \overline{D})^2. \tag{6.3}$$

The standard deviation of the mean difference is calculated as follows.

$$S_{\overline{D}} = \sqrt{S_D} \tag{6.4}$$

Then we estimate the true mean difference, also called the confidence interval, which is between two limits.

$$\overline{D} - 1.96 S_{\overline{D}} < difference < \overline{D} + 1.96 S_{\overline{D}} \tag{6.5}$$

This permits us to say with 95% confidence that the population mean difference is between $\overline{D} - 1.96S_{\overline{D}}$ and $\overline{D} + 1.96S_{\overline{D}}$. Thus, we would expect that the interval between the lower limit and the upper limit would encompass the true mean difference about 95% of the time. It is an intuitive method for comparing the difference between two groups of features by observing the intervals given certain levels of confidence.

The values of maximum difference, minimum difference, mean difference between the two classes of follicles computed from each texture feature, their standard errors, and the 95% confidence interval are presented in Table 6.1. This statistical result provides two insights. Firstly, group mean difference with a tight interval usually indicates the distribution of the two groups are similar. Secondly, given the feature values of a group, say energy feature in ovulatory follicle, the feature value of the other group can be estimated by the mean difference and confidence interval. For instance, we could expect that the true mean difference in edge density value between the two groups of follicle walls is between 13.499 and 19.4237 about 95% of the time. The mean edge density of the natural cycle group is p, thus the mean edge density of the OC cycle group (say o) can be estimated between (p - 13.499) and (p - 19.4237) with 95% confidence.

Table 6.1: Mean differences between ovulatory and anovulatory follicles.

Feature	Max Difference	Min Difference	Mean Difference	Standard Deviation	Confidence Interval(95%)
Edge Density	19.1238	14.4136	16.4614	1.5114	(13.4990, 19.4237)
Edge Contrast	21.445	17.3936	19.0259	1.4017	(16.2786, 21.7731)
Co-occurrence Energy	0.1057	0.0492	0.062	0.0184	(0.0259, 0.0980)
Co-occurrence Homogeneity	0.2331	0.1773	0.1935	0.0181	(0.1579, 0.2289)

The mean value and the standard deviation measure the variability of texture features through the maturation of an ovarian follicle. However, the validity of the statistical analysis is restricted by three factors. First, sample data should be enough so that the mean value may truly be regarded as the center of trend. Second, the selection of follicle wall areas from the original ultrasound images should be accurate. Some parts of tissues can be located easily and with high accuracy if their textures are visually detectable from ultrasound images, for example, the interior fluid area of a follicle. Some parts are difficult to select because their textures can not be observed visually.

Therefore, making use of the knowledge that follicle wall areas are homogeneous in texture will help to improve accuracy in selecting walls by hand. Finally, it is fundamental to identify the dominant follicle correctly because our assumptions and conclusions are based on dominant ovulatory and anovulatory follicles. We believe a dominant follicle always is the biggest one in the images. Thus, only the biggest follicle in an image is identified as the dominant follicle and its wall is isolated. However, it is difficult to locate the walls sometimes if there are several follicles with similar sizes in one image. Fortunately, each ultrasound image used in the thesis already has one dominant follicle identified by an expert.

6.2 Trend Analysis

The main approach used in the thesis work was the Mann-Kendall method, which is a statistical test for analyzing trends of a group of data. Mann-Kendall method tests the trends of texture features by means of locating their turning points. A turning point is defined as a point on the feature curve where a sudden change occurs. The purpose of detecting the turning point of a texture feature is to identify the existence of biological variations and locate the time at which the most distinct change appears.

6.2.1 Mann-Kendall Method

Mann proposed a method of testing for presence of trend in a sequence of numbers in 1945 [69] based on the correlation assessment by Kendall [70]. Later, Mann's test for trend was developed for estimation of the single turning point in a data series. Four basic steps of this method are given as follows.

1. Given a sequence of numbers x_t, $t = 1, 2, ..., l$, $l \leq N$, the test statistic is:

$$d_l = \sum_{i<j} sign(x_j - x_i) \tag{6.6}$$

   d_l is the number of samples in the sequence that are stochastically increasing.

2. Let $l = 1, 2, ..., N$, $E(d_l)$ and $Var(d_l)$ are the expected value and variance of d_l. Calculate the N statistics $U(d_l)$, and draw a graph of $U(d_l)$.

$$U(d_l) = (d_l - E(d_l))/\sqrt{Var(d_l)} \tag{6.7}$$

   Assume that x_1, x_2,..., x_N are independent and have the same continuous distribution, then $U(d_l)$ obeys the normal distribution $N(0, 1)$ [71].

3. Repeat 1 and 2 on a new sequence of numbers y_t, $y_t = x_{N-t+1}$, which is composed by the original sequence in reverse order. Compute the new statistic $U_{new}(d_l)$, $l = 1, 2, ..., N$. Let $U^*(d_l) = -U_{new}(d_{N-l+1})$. Draw $U^*(d_l)$ and $U(d_l)$ in one graph.

4. Find the point of intersection from the graph. If $|U| \leq 1.96$ at the intersection point, then Mann's test supports the hypothesis of a turning point at the intersection point in the sequence of numbers at a significance level of 0.05.

Turning point is an important characteristic of the feature trend. The location of turning point allows identification of the most distinct variation in the follicular development. A number of potential studies can be based on the result of turning point, for example, the prediction of an ovulatory activity by the detection of a turning point.

The Mann-Kendall method is a simple and convenient means of estimating the single turning point of a set of data. It has been successfully applied to data analysis for meteorology, such as rainfall trend analysis and climate saltation [69]. However, it has not been widely used in the analysis and prediction of physiological phenomena. The successful application of the Mann-Kendall method to the study of ovarian follicles may bring its advantage to near research areas in medical imaging.

6.2.2 Application of the Mann-Kendall Method

Four texture features involving edge density, edge contrast, co-occurrence energy and co-occurrence homogeneity were calculated and selected as good discriminators for both ovulatory and anovulatory follicles in the Chapter 5. Comparatively higher values of edge density and edge contrast were observed during the follicular development for ovulatory follicles. Higher values of energy and homogeneity feature values were observed for anovulatory follicles. In this section, the edge density, edge contrast, co-occurrence energy, and homogeneity extracted from both ovulatory follicles and anovulatory follicles were analyzed by the Mann-Kendall method.

Results from the natural cycle group are shown in Figure 6.5, in which (a) represents the application of Mann-Kendall method on the edge density feature (given $d = 1$); (b) represents the application on edge contrast feature; (c) and (d) are on co-occurrence energy and co-occurrence homogeneity texture features. The curve shown on the top of each graph represents the average feature value over time. The bottom two curves show the result of applying Mann-Kendall statistical test on the above average feature value. The solid line and dotted line in this bottom part denote statistics $U(d_l)$ and $U^*(d_l)$, respectively. Looking at graph (a), (b), (c), and (d), all the statistics $U(d_l)$ decrease with the increasing day, whereas statistics $U^*(d_l)$ have opposite trends. There is one point of intersection located between the range of $|U| \leq 1.96$. This point of intersection is called the turning point.

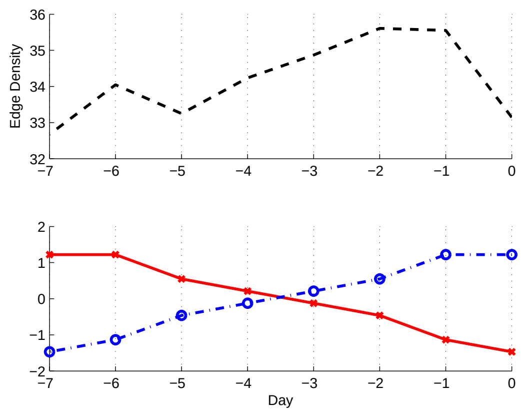

(a)

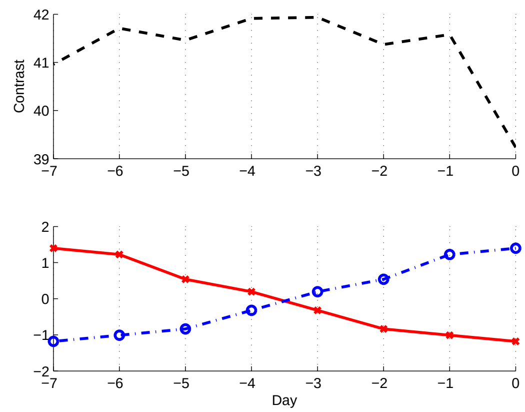

(b)

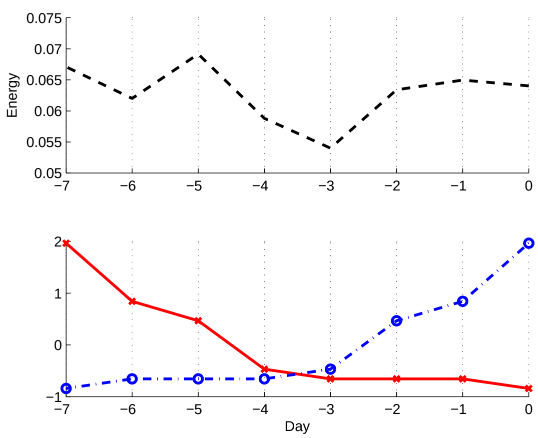

(c)

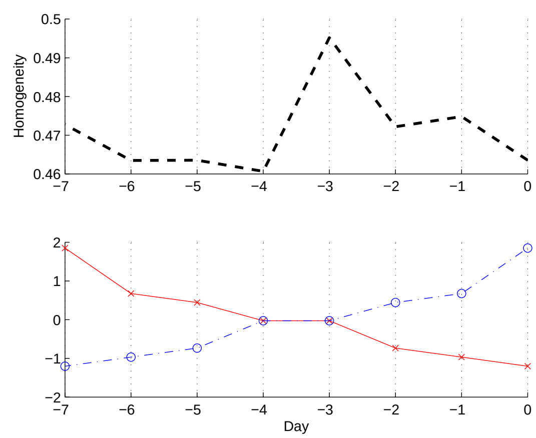

(d)

Figure 6.5: Average feature values for ovulatory follicle and the computation of statistics $U^*(d_l)$ and $U(d_l)$. Graphs (a), (b), (c), and (d) present turning point on edge density feature of normal follicle images, turning point on edge contrast feature of normal follicle images, turning point on co-occurrence energy feature of normal follicle images, and turning point on co-occurrence homogeneity feature of normal follicle images; above dotted curve is average feature value, the bottom two curves are statistics $U^*(d_l)$ and $U(d_l)$.

Compared with the average texture features on the top of each graph, the local maximum of edge density and edge contrast values are found to appear around the turning point day, that is the day between the 3rd and 4th day before ovulation (shown in (a) and (b)). From the day of turning point occurrence to the day of ovulation, edge density and edge contrast feature both have a decreasing trend, which means fewer and fewer edges are presented and thus the dominant follicle wall becomes coarser and coarser when it is close to ovulation. There appears a local minimum value on the 3rd day before ovulation for the co-occurrence energy and on the 4th day before ovulation for the co-occurrence homogeneity (shown in (c) and (d)). The turning points are also observed around these days.

The four texture features extracted from follicle images captured from women in the OC group were analyzed by the same method. Similar results were obtained. The feature curves exhibited either a maximum (edge density and edge contrast) or a minimum (co-occurrence energy and homogeneity) on the 3rd or 4th day before the appearance of the peak of E2 level. Turning points located by the Mann-Kendall method also appear around this period. This turning point is followed by a decrease in both edge density and contrast, and a increase in energy and homogeneity.

The observation of the turning point was interpreted to mean that the most distinct variations in textures of the follicle walls occur on the 3rd or 4th day before ovulation or appearance of E2 peak. It may be attributed to the cyclic changes in glycoprotein hormones in follicles. One good evidence is that the previous study of follicular dynamics [1], which employed non-image-processing approach, also detected a distinct nadir in follicle stimulating hormone (FSH) on the same time period. A nadir in FSH 3 days before the emergence of all anovulatory and ovulatory follicular waves was reported in this paper. We know that follicular waves usually emerge on the day of ovulation in women with three waves and 1 day before ovulation in women with two waves [72]. Therefore, it can be deduced that the nadir happens 3 days before ovulation in women with three waves and 4 days before ovulation in women with two waves. The time period in which the nadir in FSH was found is exactly the same as that detected by turning points of texture features.

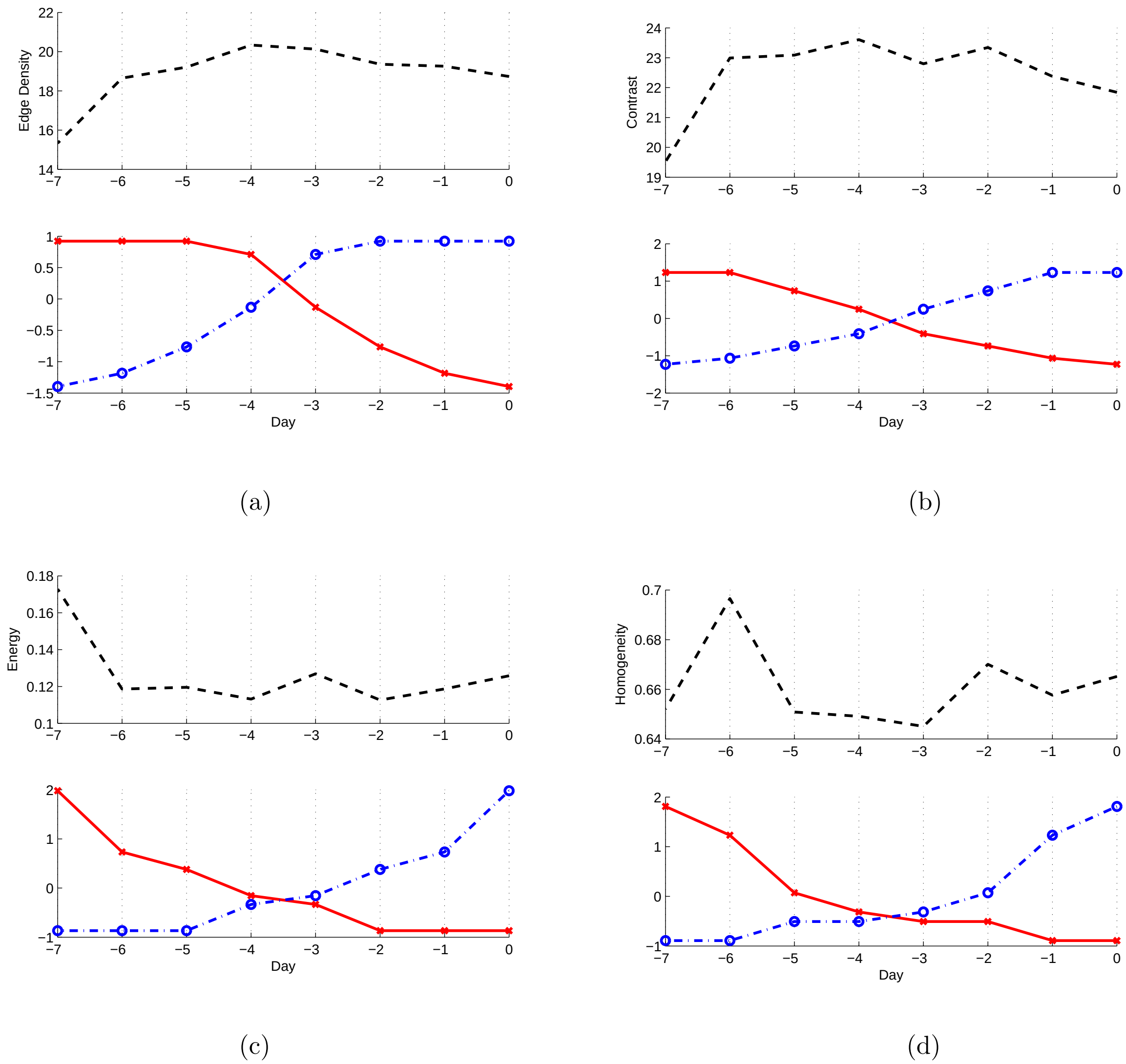

Figure 6.6: Average feature values for anovulatory follicle and the computation of statistics $U^*(d_l)$ and $U(d_l)$. Graphs (a), (b), (c), and (d) present turning point on edge density feature of anovulatory follicle images, turning point on edge contrast feature of anovulatory follicle images, turning point on co-occurrence energy feature of anovulatory follicle images, and turning point on co-occurrence homogeneity feature of anovulatory follicle images; above dotted curve is average feature value, the bottom two curves are statistics $U^*(d_l)$ and $U(d_l)$.

6.3 Summary

Turning points for the edge density, edge contrast, co-occurrence energy, and homogeneity were located between the 3rd or the 4th day before ovulation for ovulatory follicles and the 3rd or the 4th day before the appearance of E2 peak for anovulatory follicles. We may predict physiologically important end points around the times identified by the turning point analysis.

Chapter 7

Conclusion

7.1 Review of Conclusions

Our project was designed to identify and characterize echotextural features in the walls of dominant follicle obtained from women in natural menstrual cycles and women using OC. The intent was to elucidate the underlying ovarian function. Texture analysis was achieved by three steps. The first two steps, feature extraction and feature selection, provided the foundation for the later work. Feature extraction part focussed on extracting features by the texture description methods. The effective discriminators were selected in the feature selection part used for the characterization of the two types of follicles. The features were then analyzed by statistical tools. The Mann-Kendall method represents a promising new statistical approach to medical imaging data analysis, and was applied in the thesis work to detect trends and the most distinct variations of texture features over time. In conclusion,

(1) We found that co-occurrence energy, homogeneity, and correlation had consistently higher values in the horizontal direction (the direction of $0°$) compared to those in other three directions in follicle wall regions. In contrast, texture contrast for the direction of $0°$ had consistently lower values. Higher homogeneity and correlation and lower contrast values indicated a smaller amount of local texture variations in the direction of $0°$ in our images. This result was attributed to the direction from which ultrasound waves were transmitted. Ultrasound waves are from one direction and the wave frequency among the different directions are different, which was, in turn, reflected by the significant differences in echotextural features.

(2) We found that the values of co-occurrence energy and homogeneity for the follicle wall regions of anovulatory dominant follicles in women using oral contraceptives were consistently higher than the values from ovulatory dominant follicles in women in natural menstrual cycles. Moreover, in the feature spaces produced by the co-occurrence energy and homogeneity features, the two classes of follicle could be adequately separated by a discriminator function. The low homogeneity in ovulatory follicles was attributed to biological changes in the walls during the follicular development.

(3) We found that the values of edge density and edge contrast were comparatively lower for the follicle wall regions of anovulatory dominant follicles in women using oral contraceptives. The two classes of follicle were also separable in the feature spaces. The lower edge density and contrast values indicate coarser textures on the follicle walls of anovulatory follicles. This texture characteristic attributed to cellular debris during the regression of the anovulatory follicle.

(4) The maximum difference, minimum difference and group mean difference of each texture feature were computed. The results are particularly useful if more sample images are collected in future work. The mean feature value of either group can be directly approximated by the mean group difference and the confidence interval with 95% confidence.

(5) Each texture feature was found exhibiting either a maximum value (edge density and contrast) or a minimum value (co-occurrence energy and homogeneity) around the 3rd or 4th day before the day of ovulation (i.e. day 0) for ovulatory follicles, and around the 3rd or 4th day before the appearance of the peak value of E2 for anovulatory follicles. The distinct echotextural variation was attributed to cyclic changes in glycoprotein hormones.

The results in this thesis can be employed in future studies for automatic recognition of different types of ovarian follicles. We also anticipate that the thesis work has implications for applications in understanding physiologic status of follicles in women using non-invasive imaging technology.

7.2 Potential Future Extensions

The work described in this thesis may be extended.

(1) Ultrasound medical images have many non-uniform qualities. Therefore texture analyses should be performed on pre-processed images. The image pre-processing in our study was aimed at reducing the absolute intensity differences among images. A set of other pre-processing methods could be added to improve image qualities and obtain better results.

(2) The selection of appropriate texture features is dependent on particular images. Texture features selected in the thesis work may not be effective in other applications. However, the method for feature selection mentioned in this thesis is generally useful. A group of similar applications could be achieved based on this study.

(3) All the results in this thesis are obtained based on a limited amount of follicle images due to the difficulties in collecting follicular data from human ovaries. More precise variations in texture features during the follicular development would be observed if images were captured much frequently (e.g. once daily). The standard error of each feature would also be decreased. Given

enough images, a classifier can be easily generated using our selected feature discriminators to automatically separate different categories of follicles in the human ovary.

References

[1] A. R. Baerwald, G. P. Adams, and R. A. Pierson. Characterization of ovarian follicular wave dynamics in women. *Biology of Reproduction*, 69(1):1023–1031, 2003.

[2] A. R. Baerwald and R. A. Pierson. Ovarian follicular development during the use of oral contraception: A review. *Journal of Obstetrics and Gynaecology Canada*, 26(1):19–24, Jan 2004.

[3] T. Rechberger, J. Tomaszewski, A. P. Biaek, B. K. Rechberger, and P. Skorupski. Serum resistin levels in women taking combined oral contraceptives containing desogestrel or gestodene. *Contraception*, 69(6):477–480, June 2004.

[4] M. A. Renier, A. Vereechen, E. V. Herck, D. Straetmans, P. Ramaekers, J. Vanderheyden, H. Degezelle, and P. Buytaert. Dimeric inhibin serum values as markers of ovarian activity in pill-free intervals. *Contraception*, 57(1):45–48, January 1998.

[5] P. G. Crosignani, G. Testa, W. Vegetti, and F. Parazzini. Ovarian activity during regular oral contraceptive use. *Contraception*, 24(5):271–273, 1996.

[6] J. Singh, R. A. Pierson, and G. P. Adams. Ultrasound image attributes bovine ovarian follicles: Endocrine and functional correlates. *Reproduction and Fertility*, 112:19–29, 1998.

[7] R. Vassena, G. P. Adams, R. J. Mapletoft, R. A. Pierson, and J. Singh. Ultrasound image characteristics of ovarian follicles in relation to oocyte competence and follicular status in cattle. *Animal Reproduction Science*, 2360:1–17, 2002.

[8] R. A. Pierson and O. J. Ginther. Ultrasonography of the bovine ovary. *Theriogenology*, 21:495–504, 1984.

[9] J. W. Tom, R. A. Pierson, and G. P. Adams. Quantitative echotexture analysis of bovine ovarian follicles. *Theriogenology*, 50:339–346, 1998.

[10] E. Rajakoski. The ovarian follicular system in sexually mature heifers with special reference to seasonal, cyclical, and left-right variations. *Acta Endocr*, Suppl(52):7–68, 1960.

[11] R. A. Pierson and O. J. Ginther. Follicular populations during the estrous cycle in heifers. part two. time of selection of ovulatory follicle. *Animal Reproduction Science*, 16:81–95, 1988.

[12] G. Layer, I. Zuna, A. Lorentz, H. Zerban, U. Haberkorn, P. Bannasch, G. V. Kaich, and U. Rath. Computerized ultrasound B-Scan texture analysis of experimental fatty liver disease: Influence of total lipid content and fat deposit distribution. *Ultrasonic Imaging*, 12:171–188, 1990.

[13] J. M. Thijssen, B. J. Oosterveld, P. C. Hartman, and G. J. E. Rosenbusch. Correlations between acoustic and texture parameters from RF and B-Model liver echograms. *Ultrasound in Med and Biol*, 19(1):13–20, 1993.

[14] O. Basset, Z. Sun, J. L. Mestas, and G. Gimenez. Texture analysis of ultrasonic images of the prostate by means of co-occurrence matrices. *Ultrasonic Imaging*, 15:218–237, 1993.

[15] K. G. Kim, S. W. Cho, S. J. Min, J. H. Kim, B. G. Min, and K. T. Bea. Computerized scheme for assessing ultrasonographic features of breast masses. *Academic Radiology*, 12(1):58–66, 2005.

[16] E. A. Stewart, W. M. W. Gedroyc, C. M. C. Tempany, B. J. Quade, Y. Inbar, T. Ehrenstein, A. Shushan, J. T. Hindley, R. D. Goldin, and M. David. Focused ultrasound treatment of uterine fibroid tumors: Safety and feasibility of a noninvasive thermoablative technique. *American Journal of Obstetrics and Gynecology*, 189:48–54, July 2003.

[17] A. U. Bako, S. Morad, and W. A. Atiomo. Polycystic ovary syndrome: An overview. *Reviews in Gynaecological Practice*, 5:115–122, June 2005.

[18] K. Mueller, T. Welsh, W. Zhu, J. Meade, and N. Volkow. Brainminer: A visualization tool for ROI-based discovery of functional relationships in the human brain. *New Paradigms in Information Visualization and Manipulation (NPIVM) 2000*, pages 481–485, November 2000.

[19] T. Welsh, K. Mueller, W. Zhu, N. Volkow, and J. Meade. Graphical strategies to convey functional relationships in the human brain: A case study. *12th IEEE Visualization 2001 Conference (VIS 2001)*, pages 481–485, October 2001.

[20] J. K. Jain, F. Ota, and D. R. Mishell. Comparison of ovarian follicular activity during treatment with a monthly injectable contraceptive and a low-dose oral contraceptive. *Contraception*, 61(3):195–198, March 2000.

[21] M. Broome, J. Clayton, and K. Fotherby. Enlarged follicles in women using oral contraceptives. *Contraception*, 52:13–16, 1995.

[22] O. J. Ginther, K. Kot, L. J. Kulick, and M. C. Wiltbank. Sampling follicular fluid without altering follicular status in cattle: Oestradiol concentrations early in a follicular wave. *Reproduction and Fertility*, 109:181–186, 1997.

[23] J. Singh, G. P. Adams, and R. A. Pierson. Promise of new imaging technologies for assessing ovaian function. *Animal Reproduction Science*, 78:371–399, 2003.

[24] U. Manivannan, G. E. Sarty, H. Sirounis, J. Singh, G. P. Adams, and R. A. Pierson. Physiologic classification of bovine ovarian follicles with wavelet packet texture analysis. *Proceedings of SPIE*, 3661:1238–1245, 1999.

[25] G. E. Sarty, W. Liang, M. Sonka, and R. A. Pierson. Semiautomated segmentation of ovarian follicular ultrasound images using a knowledge-based algorithm. *Ultrasound in Med and Biol*, 24:27–42, 1997.

[26] J. L. Schwartz, M. D. Creinin, H. C. Pymar, and L. Reid. Predicting risk of ovulation in new start oral contraceptive users. *Obstetrics and Gynecology*, 99(2):177–182, February 2002.

[27] R. N. Sutton and E. L. Hall. Texture measures for automatic classification of pulmonary disease. *IEEE Transactions on Computers*, C(21):667–676, 1972.

[28] G. H. Landeweerd and E. S. Gelsma. The use of nulear texture parameters in the automatic analysis of leukocytes. *Pattern Recognition*, 10:57–61, 1978.

[29] B. Georgescu and C. M. Christoudias, Robust Image Understanding Laboratory, Rutgers University, http://www.caip.rutgers.edu/riul/.

[30] J. T. M verhoeven and J. M. Thijssen. Improvement of lesion detectability by speckle reduction filtering: A quantitative study. *Ultrasonic Imaging*, 15:181–204, 1993.

[31] G. Finet, C. Cachard, P. Delachartre, E. Maurincomme, and J. Beaune. Artifacts in intravascular ultrasound imaging during coronary artery stent implantation. *Ultrasound in Med and Biol*, 6:793–802, 1998.

[32] G. Castellano, L. Bonilha, L. M. Li, and F. Cendes. Texture analysis of medical images. *Clinical Radiology*, 59:1061–1069, 2004.

[33] R. M. Haralick and K. Shanmugam. Textural feature for image classification. *IEEE Transactions On Systems, Man, And Cybernetics*, SMC–3(6):610–619, November 1980.

[34] L. V. Gool, P. Dewaele, and A. Oosterlinck. Texture analysis anno 1983. *Computer Vision, Graphics, and Image Processing*, 29:336–357, 1985.

[35] M. Sonka, V. Hlavac, and R. Boyle. *Image Processing, Analysis and Machine Vision*. Brooks/Cole, A Division of Thomson Asia Pte Led, USA, 2 edition, 2002.

[36] J. Scharcanski and C. T. J. Dodson. Stochastic texture image estimators for local spatial anisotropy and its variability. *IEEE Transactions on Instrumentation and Measurement*, 49(5):271–273, 2000.

[37] S. Bonnevay. Texture features extraction with the help of regional extremality coding. *Recpad*, March 1998.

[38] S. Mavromatis, J. Boi, R. Bulot, and J. Sequeira. Texture analysis using directional local extrema. *ICCVG*, pages 25–29, September 2002.

[39] L. M. Linnett and A. J. Richardson. Texture segmentation using directional operators. *Proceedings of the 1990 International Conference on Acoustics, Speech, and Signal Processing*, pages 2309–2312, 1986.

[40] M. Tuceryan. *The Handbook of Pattern Recognition and Computer Vision*, chapter 2.1, pages 207–248. Texture Analysis. World Scientific Co., second edition, 1998.

[41] G. C. Cross and A. K. Jain. Markov random field texture models. *IEEE Transactions on Pattern Analysis and Machine Intelligence*, PAMI(5):25–39, 1983.

[42] R. Chellappa and S. Chatterjee. Classification of textures using Gaussian Markov random fields. *IEEE Transactions on Acoustic, Speech, and Signal processing*, ASSP(33):959–963, 1985.

[43] A. Pentland. Fractal-based description of natural scenes. *IEEE Transactions on Pattern Analysis and Machine Intelligence*, pages 661–674, 1984.

[44] J. Besag. Spatial interaction and the statistical analysis of lattice systems. *Journal of the Royal Statistical Society*, 36:192–236, 1974.

[45] R. L. Kashyap. *Handbook of Pattern Recognition and Image Processing*. Image Modelling. Academic Press, 1986.

[46] R. Chellappa and A. K. Jain. *Markov Random Fields: Theory and Application*. Academic Press, Boston, MA, 1993.

[47] D. Marr. *Vision: a computational investigation into the human representation and processing of visual information*. W.H. Freeman and Co., SanFrancisco, 1982.

[48] H. Voorhees and T. Poggio. Detecting textons and texture boundaries in natural images. *International Conference on Computer Vision*, 24:250–258, 1987.

[49] M. Tuceryan and A. K. Jain. Texture segmentation using Voronoi polygons. *IEEE Transactions on Pattern Analysis and Machine Intelligence*, PAMI-12:211–216, February 1990.

[50] F. Tomita and S. Tsuji. *Computer analysis of visual textures*. Kluwer Academic Publishers, Boston, 1990.

[51] J. Serra. *Image Analysis and Mathematical Morphology*. London Academic Press, 1982.

[52] T. H. Hong, M. Shneier, and A. Rosenfeld. Border extraction using linked edge pyramids. *IEEE Transactions on Systems, Man and Cybernetics*, 12(5):660–668, 1982.

[53] K. I. Laws. Texture energy measures. *Proc.Image Understanding Workshop*, pages 41–51, 1979.

[54] R. Wang, A. R. Hanson, and F. M. Riseman. Texture analysis based on local standard deviation of intensity. *IEEE Computer Society Conference on Computer Vision and Pattern Recognition*, pages 482–488, June 1986.

[55] L. S. Davis and A. Mitiche. Edge detection in textures. *Computer Graphics and Image Processing*, 12:25–39, 1980.

[56] T. Randen and J. Husoy. Filtering for texture classification: A comparative study. *IEEE Transactions on Pattern Analysis and Machine Intelligence*, 21(4):291–310, April 1999.

[57] P. Kruizinga, N. Petkov, and S. E. Grigorescu. Comparison of texture features based on gabor filters. *Proceedings of the 10th International Conference on Image Analysis and Processing*, pages 142–147, September 1999.

[58] R. Jenssen and T. Eltoft. Independent component analysis for texture segmentation. *Pattern Recognition*, 36:2301–2315, 2003.

[59] S. G. Mallat. A theory of multirresolution signal decomposition: The wavelet representation. *IEEE Transactions on Pattern Analysis and Machine Intelligence*, 11(7):674–693, 1989.

[60] S. Li, J. T. Kwok, H. Zhu, and Y. Wang. Texture classification using the support vector machines. *Pattern Recognition Letters*, 36:2883–2893, 2003.

[61] G. M. Haley and B. S. Manjunath. Rotation-invariant texture classification using a complete space-frequency model. *IEEE Transactions on Image Processing*, 8(2):255–269, Feb 1999.

[62] T. Chen, Y. J. Hsu, X. Liu, and W. Zhang. Principle component analysis and its variants for biometrics. *IEEE International Conference on Image Processing*, 1:22–25, Sep 2002.

[63] K. Y. Yeung and W. L. Ruzzo. Principle component analysis for clustering gene expression data. *Bioinformatics*, 17(9):763–774, 2001.

[64] A. M. Posadas, F. Vidal, F. Migual, G. Alguacil, J. Pena, J. M. Ibanez, and J. Morales. Spatial-temporal analysis of a seismic series using the principal components method: The antequera series. *Geophysical Research Letters*, 98(B2):1923–1932, 1993.

[65] T. I. Urbancic, C. I. Trifu, and R. P. Young. Microseismicity derived fault planes and their relationship to focal mechanism, stress inversions and geologic data. *Geophysical Research Letters*, 20(22):2475–2478, 1993.

[66] M. P. Prince, S. C. Maxwell, and T. I. Urbancic. Identifying fracture patterns in microseismic data sets. Technical report, 2003 CSEG Conference, 2003.

[67] T. Haenselmann and W. Effelsberg. Texture resynthesize using principle component analysis. In *SPIE Human Vision and Electronic Imaging VII*. SPIE The International Society for Optical Engineering, January 2002.

[68] G. A. F. Seber. *Multivariate Observations*. Wiley Series in Probability and Mathematical Statistics. Wiley, 1984.

[69] R. Sneyers. On the statistical analysis of series of observations. Technical note, World Meteorological Organization Technical Note, 1990.

[70] N. L. Johnson, C. B. Read, and S. Kotz. *Encyclopedia of Statistical Sciences*. New York : Wiley, 1981.

[71] J. Xiang and J. Shi. *Statistical Methods of Data Analysis in Non-linear System*. Science Press, China, 1997.

[72] A. R. Baerwald, Hon, G. P. Adams, and R. A. Pierson. A new model for ovarian follicular development during the human menstrual cycle. *Fertility and Sterility*, 80(1):116–122, July 2003.

Appendix A
GLCM Texture Features

Haralick et. al. [33] suggested a set of 14 texture features which can be extracted from normalized GLCM. They are defined as follows.

$$Energy = \sum_{i=1}^{N_g} \sum_{j=1}^{N_g} p_d^2(i,j) \tag{A. 1}$$

$$Contrast = \sum_{n=0}^{N_g-1} n^2 (\sum_{i=1}^{N_g} \sum_{j=1}^{N_g})_{|i-j|=n} p_d(i,j) \tag{A. 2}$$

$$Correlation = \frac{\sum_{i=1}^{N_g} \sum_{j=1}^{N_g} (i-\mu_i)(i-\mu_i) p_d(i,j)}{\sigma_i \sigma_j} \tag{A. 3}$$

$$Variance = \sum_{i=1}^{N_g} \sum_{j=1}^{N_g} (i-\mu_i)(j-\mu_j) p_d(i,j) \tag{A. 4}$$

$$Homogeneity = \sum_{i=1}^{N_g} \sum_{j=1}^{N_g} \frac{p_d(i,j)}{1+|i-j|} \tag{A. 5}$$

$$SumAverage = \sum_{n=2}^{2N_g} n \sum_{|i+j|=n} p_d(i,j) \tag{A. 6}$$

$$SumVariance = \sum_{n=2}^{2N_g} (n-f)^2 \sum_{|i+j|=n} p_d(i,j) \tag{A. 7}$$

$$SumEntropy = f = -\sum_{n=2}^{2N_g} \sum_{|i+j|=n} p_d(i,j) \log \sum_{|i+j|=n} p_d(i,j) \tag{A. 8}$$

$$Entropy = -\sum_{i=1}^{N_g} \sum_{j=1}^{N_g} p_d(i,j) \log p_d(i,j) \tag{A. 9}$$

$$DifferenceVariance = varianceof \sum_{|i-j|=n} p_d(i,j) \tag{A. 10}$$

$$DifferenceEntropy = -\sum_{n=0}^{N_g-1} \sum_{|i-j|=n} p_d(i,j) \log \sum_{|i-j|=n} p_d(i,j) \tag{A. 11}$$

$$InformationMeasuresofCorrelation1 = \frac{HXY - HXY1}{max(HX, HY)} \tag{A. 12}$$

$$InformationMeasuresofCorrelation2 = (1 - exp[-2(HXY2 - HXY)])^{1/2} \tag{A. 13}$$

where HX and HY are entropies of $p_d(i)$ and $p_d(j)$, and

$$HXY1 = -\sum_i \sum_j p_d(i,j) \log p_d(i) p_d(j) \tag{A. 14}$$

$$HXY2 = -\sum_i \sum_j p_d(i) p_d(j) \log p_d(i) p_d(j) \tag{A. 15}$$

$$HXY = -\sum_i \sum_j p_d(i,j) \log p_d(i,j) \tag{A. 16}$$

$$MaximalCorrelationCoefficient = (SecondlargesteigenvalueofQ)^{1/2} \tag{A. 17}$$

where

$$Q(i,j) = \sum_k \frac{p_d(i,k)p_d(j,k)}{p_d(i)p_d(j)} \tag{A. 18}$$

These 14 features are not independent. In practice, a feature selection procedure should be applied to select a subset of the features.

Appendix B
Sample Ultrasound Ovarian Follicle Images

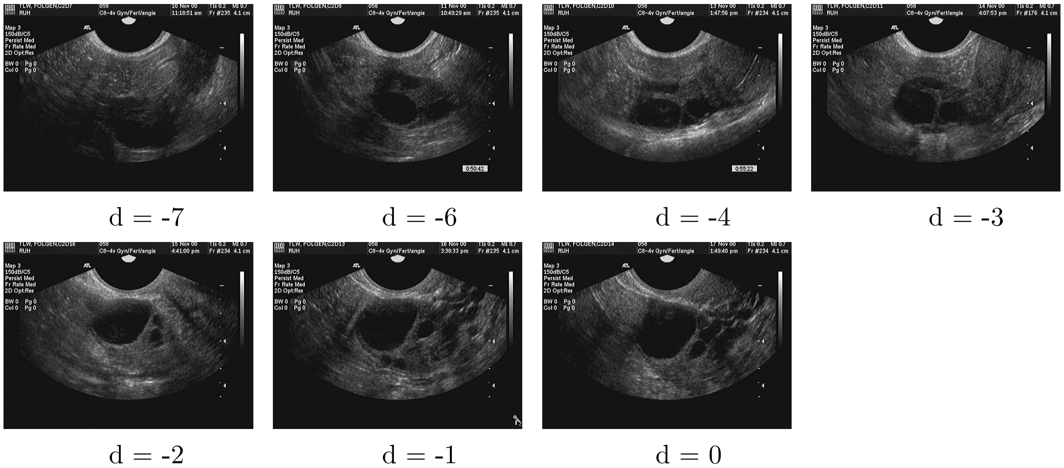

Figure B. 1: Original ultrasound images for TLW for the 7 days before ovulation

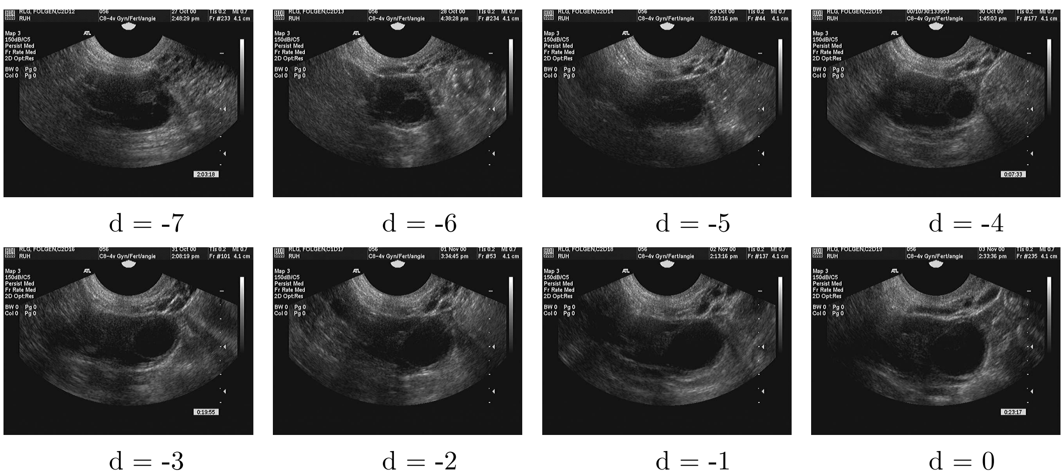

Figure B. 2: Original ultrasound images for RLG for the 8 days before ovulation

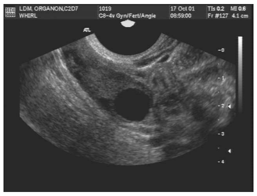
d = -5

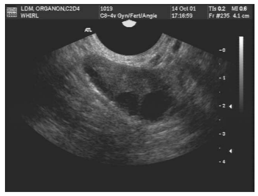
d = -4


d = -2

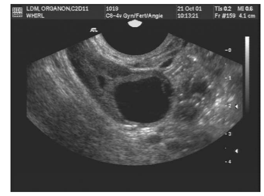
d = -1

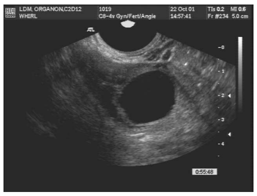
d = 0

Figure B. 3: Original ultrasound images for LDM for the 5 days before appearance of E2 peak


d = -7


d = -6

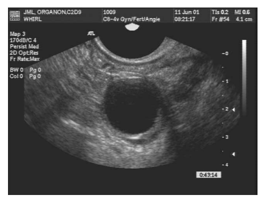
d = -5

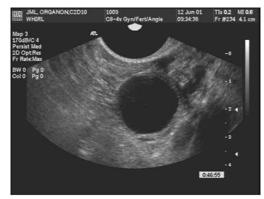
d = -4

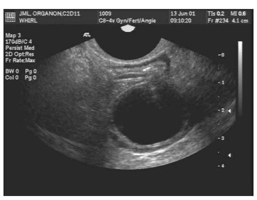
d = -3


d = -2

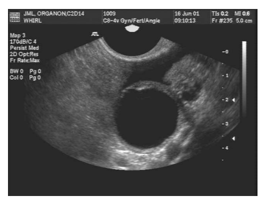
d = 0

Figure B. 4: Original ultrasound images for JML for the 7 days before appearance of E2 peak